IEEE Access
Multidisciplinary | Rapid Review | Open Access Journal

Received 3 December 2022, accepted 11 December 2022, date of publication 15 December 2022,
date of current version 12 January 2023.

Digital Object Identifier 10.1109/ACCESS.2022.3229893

RESEARCH ARTICLE

Power Quality Compensation Strategy of MMC-UPQC Based on Passive Sliding Mode Control

CHANG JIANG AND SHAOHUA ZHANG
School of Mechatronic Engineering and Automation, Shanghai University, Baoshan, Shanghai 200444, China
Corresponding author: Chang Jiang (jackupup2022@163.com)

ABSTRACT While the unified power quality conditioner based on modular multilevel converter (MMC-UPQC) can be used for recovering power quality of voltage and current in high voltage grids, it is difficult to manage the power quality when the grid voltage imbalance is large. In this paper, a passivity-based control (PBC) combined with sliding mode control (SMC) is proposed for MMC-UPQC to improve the power quality under the unbalance of grid voltage in power systems. First, according to the structure of MMC-UPQC, the equivalent mathematical model is presented for unbalanced power grids. Second, the detection quantity is separated without phase-locked loop using a method of positive and negative sequence separation. Furthermore, a passive sliding mode control (PSMC) strategy is designed and applied to a multi-level and high voltage power quality compensation system. The proposed controller can improve the control accuracy of system parameters, response speed, and compensation effectiveness. Finally, the MATLAB/Simulink simulation and the real time laboratory (RT-LAB) based hardware-in-the-loop (HIL) experimental results show that the proposed PSMC strategy can compensate voltage and current rapidly and accurately, and the controller has strong robustness against system parameter changes.

INDEX TERMS Modular multilevel converter, passivity-based control, sliding mode control, unbalanced grid voltage, unified power quality regulator.

I. INTRODUCTION

Since the advent of the modular multilevel converter (MMC) [1], it has been increasingly studied and applied in various fields. Specifically, large level numbers and common direct current (DC) side make the MMC very suitable for application in DC transmission [2], [3]. Nowadays, because of its multi-module characteristics, MMC has been used in active filters, and can compensate well for harmonics of current and voltage. In recent years, many power electronic devices have been put into operation, accompanied by temporary swell and fall of grid voltage, flicker, fluctuation and other non-ideal conditions, resulting in the degradation of power quality. Unified power quality conditioner (UPQC) consists of the series side and the shunt side, which can realize compensation for voltage and current. And the flexibility and compensation versatility of UPQC are widely used and studied to improve power quality, but UPQC is difficult to apply under high voltage grids due to the large voltage amplitude of medium and high-power grids. Fortunately, MMC can be applied to UPQC in medium and high voltage scenarios due to its high voltage withstand level and low switching frequency [5]. The series and shunt converters that make up the UPQC are used to recover the voltage and current quality, respectively. Through the coordinated control, MMC-UPQC can recover power quality and maintain stable operation of grid voltage in power systems. However, when the power grid is unbalanced, especially in the medium and high voltage conditions, voltage and current distortions are severe and MMC-UPQC has difficulty in achieving a satisfactory compensation effect.

The associate editor coordinating the review of this manuscript and approving it for publication was Shihong Ding.

Grid unbalance is a very common grid state, so it is necessary to study the control strategy for MMC-UPQC under the unbalanced grid.

Recently, many scholars carry out researches on the control effects of different control strategies. In [6] and [7], linear proportional-integral (PI) control method is adopted to UPQC. However, when the system receives disturbances, PI is hard to obtain good static performance and the control parameters are difficult to determine. In [8], the circulating current suppression control and capacitance average voltage control are not included in the control system. Therefore, the output voltage becomes unstable without capacitance voltage control. Some practical examples of improved PI control can be found in previous studies [9], [10]. However, these improved controllers are computationally complex. In [11] and [12], a shunt compensation control method for MMC-UPQC is presented, which can effectively compensate the current. But it does not involve the recovering effect of the voltage falling on the series side. Limited current coordinated control is adopted to effectively solve the problem of voltage sag on the series side. However, it does not deal with other situations well and the robustness is poor [13]. Passivity-based control (PBC) is designed to restore power quality [14]. But when the system parameters change, PBC has poor adaptability. In addition, the controller is not suitable for unbalanced power systems in high voltage grids. Passive sliding mode control (PSMC) is presented in [15]. Although PSMC improves the compensation method for negative sequence currents on the series side, it does not address the compensation method in the case of voltage and current imbalance. A new super-twisting-like fractional controller for surface-mounted permanent magnet synchronous motor system is proposed to improve the control performance, which replaces the discontinuous switching function with a non-smooth term [16]. Hysteresis current control strategy for MMC has fast response speed, but in the design process, the slope of the current is replaced by the slope of sampling period approximately [17]. Therefore, the controller is not precise, so the error is large. A coordinated control used to control the power quality in grid voltage balance is proposed in [18] and [19], however the effect is not good. An adaptive fuzzy logic controller based on series hybrid active power filter (SHAPF) is proposed in [20]. Because the number of sub-modules (SMs) in MMC-UPQC is large and the controller needs to control many switches, control accuracy and effect of fuzzy control methods in [20] are reduced. Therefore, this control method is difficult to apply to MMC-UPQC.

In the case of grid imbalance, the control strategy for MMC-UPQC still has some problems, such as slow reaction speed, poor compensation effect and poor robustness, etc. Moreover, control objectives are difficult to achieve in the presence of grid imbalances. Some control strategies can only compensate voltage or current individually but cannot improve both voltage and current quality.

To realize the nonlinear control of power electronic devices, the PBC theory has been applied to a lot of inverters [21]. Currently, PBC strategies have been applied to power electronic devices, and has achieved good control results [10], [22], [23]. PBC discusses the stability of the controlled object from the perspective of energy shaping and injection damping. Without complicated transformations, the system can be controlled by selecting the suitable energy function and the injection damping. On the other hand, sliding mode control (SMC) is a commonly used and discontinuous nonlinear control method [24]. It can be used in a dynamic process based on the current state of a constantly changing system (such as deviation and their derivatives of each order). However, PBC and SMC have their own shortcomings. Due to the high dependence of PBC on the mathematical model and system parameters of the system, it is difficult to achieve optimal results. On the other hand, SMC has jitter, so it is hard to stabilize. Some scholars combine SMC and other methods to control power electronic devices [25], [26]. However, these control methods are not suitable for high voltage and multi-level situations. Some scholars have used an adaptive SMC strategy to solve the problems for a class of nonlinear singular time-varying delay systems [27]. A generalized proportional integral is adopted to observer super-twisting sliding mode controller to estimate the time-varying disturbance [28]. In order to take full use of the advantages of PBC and SMC, this paper combines the two controls to design PSMC. The PSMC, a kind of control strategy for variable structure control systems, purposefully changes the system to operate on a predetermined ”sliding mode” state trajectory based on the current state of the system. Thus, PSMC is insensitive to parameter changes and the disturbance, allowing the controller resistant to interference. Sliding mode can resist the influence of external disturbances and internal parameters on the system. Therefore, PSMC can adapt to changes in the system and solve the problem of poor control effect from PBC due to parameter changes.

From existing literature, we observe that there are still some limitations in these studies which can be given as follows:

(1) To date, studies related to MMC-UPQC mainly focus on the control effect when voltage sags and swells. And several common situations under unbalanced grids, such as load switching and harmonic injection, are not considered.

(2) Studies on power quality of UPQC focus on the management of shunt-side currents and harmonics, while the design of controllers for voltage quality on series side is still in its fledgling stages.

(3) Following the decarbonizing policies around the world, large scale of renewable energy sources will enter the grid and subsequently occupy a very high proportion. Facing increasing fluctuations and harmonics from renewable energy equipment, the conventional control methods, such as PI control, SMC and PBC, are difficult to adapt to changes in system parameters and achieve satisfactory control performance.

In observing existing limitations, we focus on offering the following main contributions in this paper.

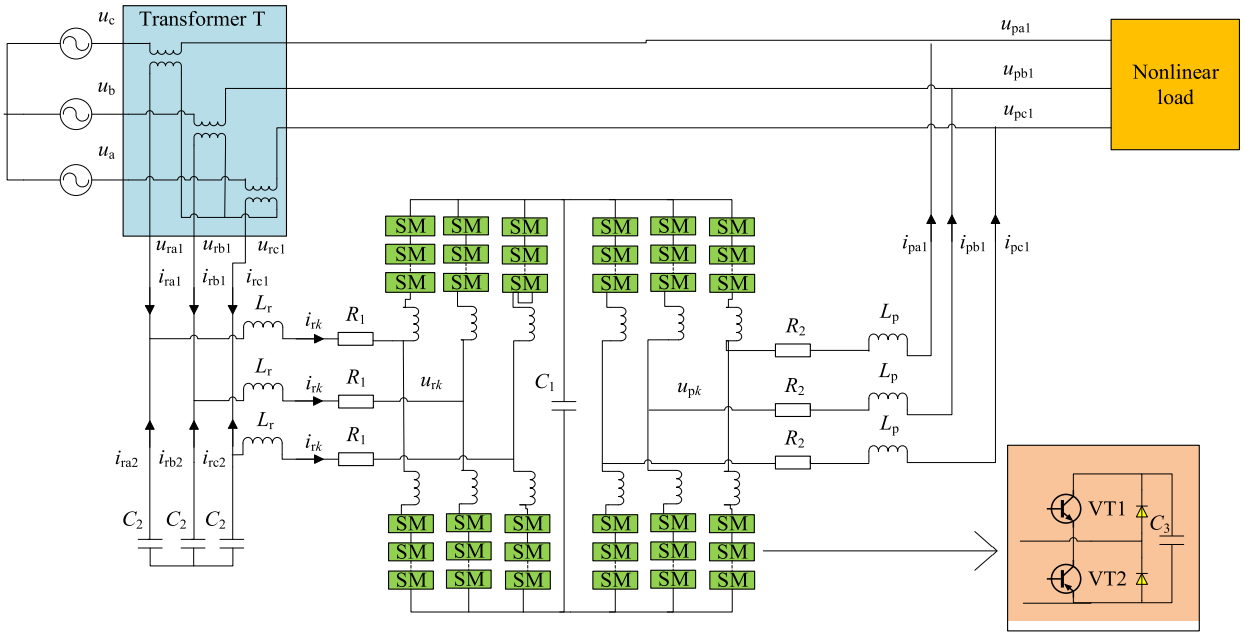

FIGURE 1. The main circuit topology of MMC-UPQC.

(1) The proposed PSMC for MMC-UPQC under grid unbalance can cope with the emergence of more complex imbalances in the grid. By combining DC-link capacitance voltage control and the coordination control for MMC-UPQC, problems such as the complex parameters of the integrated system and the slow reaction speed can be tackled. In addition, the proposed PSMC can quickly restore the voltage and current quality, ensuring the power quality effectively. The feasibility and effectiveness of the proposed control system are verified by MATLAB/Simulink simulation and real time laboratory (RT-LAB) based hardware-in-the-loop (HIL) test results with comparisons to the PI and PBC.

(2) Series-side voltage control that is not included in other studies is considered in this paper. We not only consider the control effect on shunt-side MMC, but also pay much attention to the change of voltage quality on series side. The design process of the series-side controller will be described in detail in Section IV, and its control effects are shown in Sections V and VI.

(3) PSMC can maintain stability during sudden unbalance condition. Both load voltage on series side and grid current on shunt side can be recovered to less than 5% harmonic distortion rate under PSMC control. Compared with PBC and PI, the overshoot is smaller and the recovered waveform is closer to sine wave under PSMC.

II. STRUCTURE OF MMC-UPQC

A. TOPOLOGY OF MMC-UPQC

The main circuit topology of the MMC-UPQC is shown in Fig. 1. In this paper, the back-to-back connection method is used between series-side MMC and shunt-side MMC due to its stable structure. Meanwhile, the DC-link is composed of a large capacitance, which can provide enough energy to MMC-UPQC. In general, the two MMC converters on series and shunt sides are close to the grid side and the load side, respectively. The MMC on the series side is connected to the grid system through transformer T, capacitors, and inductors, which is used to compensate the voltage. So, the load voltage is restored to the sinusoidal waveform by MMC on the series side when voltage transient sag, transient swell, harmonics, and flashes occur in the grids. Similarly, MMC on the shunt side is needed to compensate the current. Due to the existence of non-linear load, current on the load side often contains lots of harmonics. To prevent harmonic currents from entering the grid and deteriorating power quality, the MMC on shunt side generates compensation currents to offset harmonics.

As shown in Fig. 1, u_a, u_b, u_c are grid three phase voltage. In addition, u_{rk} and u_{pk} represent output voltage of MMCs on series side and shunt side. u_{rk1} is transformer primary side voltage and u_{pk1} is line voltage. The MMC current i_{rk} flows into the series side, where i_{rk1} and i_{pk1} are the line currents of the series and shunt sides respectively. The current i_{rk2} flows into the series side capacitance. There are circuit inductors L_r, L_p and circuit resistors R_1, R_2 between the two MMCs and the grids, respectively. C_1 is DC side capacitance for the middle of the two converters, while C_2 is shunt capacitance for series side. MMC-UPQC is divided into upper and lower bridge arms per phase and consists of six bridge arms in total. The N-module MMC contains $2N$ SMs and 1 inductor per phase, meaning that there are N SMs in each of the upper and lower bridge arms. Ideally, N-module MMC can output $2N + 1$ number of levels, and the harmonics will be smaller as the number of levels increases. Each SM consists of 2 half-bridge insulated gate bipolar transistors (IGBT) and 1 capacitance, where the capacitor mainly plays the role of charging and discharging. Each SM has 3 operating states of

input, excision, and locking. In the input state, thyristor VT_1 turns on and VT_2 turns off; in the resection state, thyristor VT_1 turns off and VT_2 turns on; in the lock state, thyristors VT_1 and VT_2 are off.

B. MATHEMATICAL MODEL OF MMC-UPQC

According to the equivalent circuit of the MMC and Kirchhoff's law, mathematical model on the series side can be obtained from Fig. 1 as follows

$$u_{rk1} = u_{rk} + L_{req}\frac{di_{rk}}{dt} + R_1 i_{rk} \tag{1}$$

where, u_{rk} is the series side MMC output voltage of phase k (k = a, b, c). The series side equivalent inductance L_{req} is the sum of the line inductance on series side and the half of bridge arm inductance. R_1 is line resistance on the series side and i_{rk} is line current on the series side.

Considering the presence of transformers on the series side, when the voltage ratio is m, $u_{rk1} = mu_{rk2}$.

In the same way, we can get mathematical model on the shunt side given as

$$u_{pk1} = u_{pk} + L_{peq}\frac{di_{pk}}{dt} + R_{2ipk} \tag{2}$$

where, u_{pk1} represents line side voltage. u_{pk} and L_{peq} are output voltage of MMC shunt side and equivalent inductance. R_2 is line resistance on shunt side and i_{pk} is line current on shunt side.

According to (1) and (2), the mathematical models for MMC-UPQC in the dq rotating coordinate system can be deduced as

$$\begin{cases} u_{rd1} = u_{rd} + L_{req}\frac{di_{rd}}{dt} + R_{1ird} - \omega L_{req} i_{rq} \\ u_{rq1} = u_{rq} + L_{req}\frac{di_{rq}}{dt} + R_{1irq} + \omega L_{req} i_{rd} \end{cases} \tag{3}$$

$$\begin{cases} u_{pd1} = u_{pd} + L_{peq}\frac{di_{pd}}{dt} + R_{2ipd} - \omega L_{peq} i_{pq} \\ u_{pq1} = u_{pq} + L_{peq}\frac{di_{pq}}{dt} + R_{2ipq} + \omega L_{peq} i_{pd} \end{cases} \tag{4}$$

where, grid fundamental angular velocity ω meets $\omega = 2\pi f$, and frequency f equals 50Hz.

C. DUAL-LOOP PI CONTROL STRATEGY FOR MMC-UPQC

Currently, PI control is the most widely used in industrial control due to its simple structure and mature products. And PI control is a traditional and classic control method, which is currently used in most equipment. To highlight and demonstrate the benefits of PSMC for MMC-UPQC, a comparison between PSMC and PI dual-loop control is presented in Section V.

The PI control for MMC-UPQC used in this paper is a two-loop vector control based on the dq coordinate system. The outer ring is the voltage loop, and the inner ring is the current loop. The function of the outer loop controller is to obtain target quantities of the current inner loop based on the set voltage reference quantities on the d-axis and q-axis. On the other hand, the function of the inner loop current controller is to be able to quickly decouple the current components of the d and q axes. In addition, the inner loop can quickly follow the given and determine the magnitude of the differential mode voltage of the upper and lower bridge arms of the MMC.

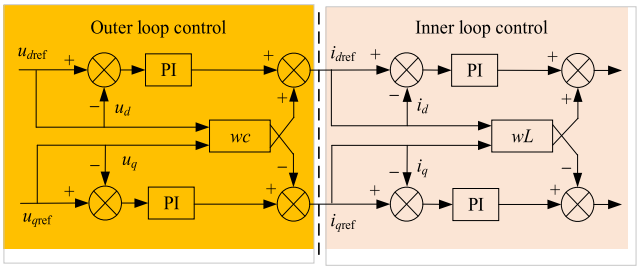

FIGURE 2. PI dual loop control structure of MMC-UPQC.

The PI double loop control structure of MMC-UPQC is shown as Fig. 2. The outer ring generates current reference quantities i_{dref} and i_{qref}, which then goes to the inner loop for comparison with the detected quantities i_d and i_q. Then, the modulation signal is set to follow the target values u_{dref} and u_{qref} through the inner loop control.

In Fig. 2, u_d and u_q are voltage components of the dq rotating coordinate system. u_{dref} and u_{qref} represent the set voltage target values.

PI control has the defects of slow reaction speed, large overshoot and low recovery degree, resulting in poor results. In addition, the PI control structure is too simple to realize the coordinated control for MMC-UPQC. In that case, the voltage and current quality problems cannot be solved simultaneously. Therefore, we present a PSMC strategy for MMC-UPQC. In this paper, the PSMC strategy is designed for the inner loop. Compared with the PI controller, the PSMC can improve the performance of MMC-UPQC and achieve better compensation effect of power quality.

III. NEW CONTROL STRATEGY FOR INTEGRATED MANAGEMENT OF MMC-UPQC

For achieving the goal of comprehensive treatment, the core idea of PSMC for MMC-UPQC is presented as follows: in order to deal with voltage and current problems in three-phase unbalance and improve power quality, the detection values are first divided into positive and negative sequences. PSMC is used in the current inner loop control. MMC on series side is connected to the line through the transformer to compensate the grid voltage and bring the voltage to the specified value. When a voltage or current failure occurs in the power system, the entire controller provides compensation voltage through the series side of MMC-UPQC. In order to offset the harmonic current of the nonlinear load and prevent the harmonic from entering the grid, compensation current is generated by the shunt side MMC.

The new control system structure of MMC-UPQC is shown as Fig. 3. In Fig. 3, i_d^+, i_q^+, i_d^-, i_q^- are the positive and negative sequence components of the dq axis current. In addition, u_{cir} and u_{dc} denote the output control quantity of the circulation

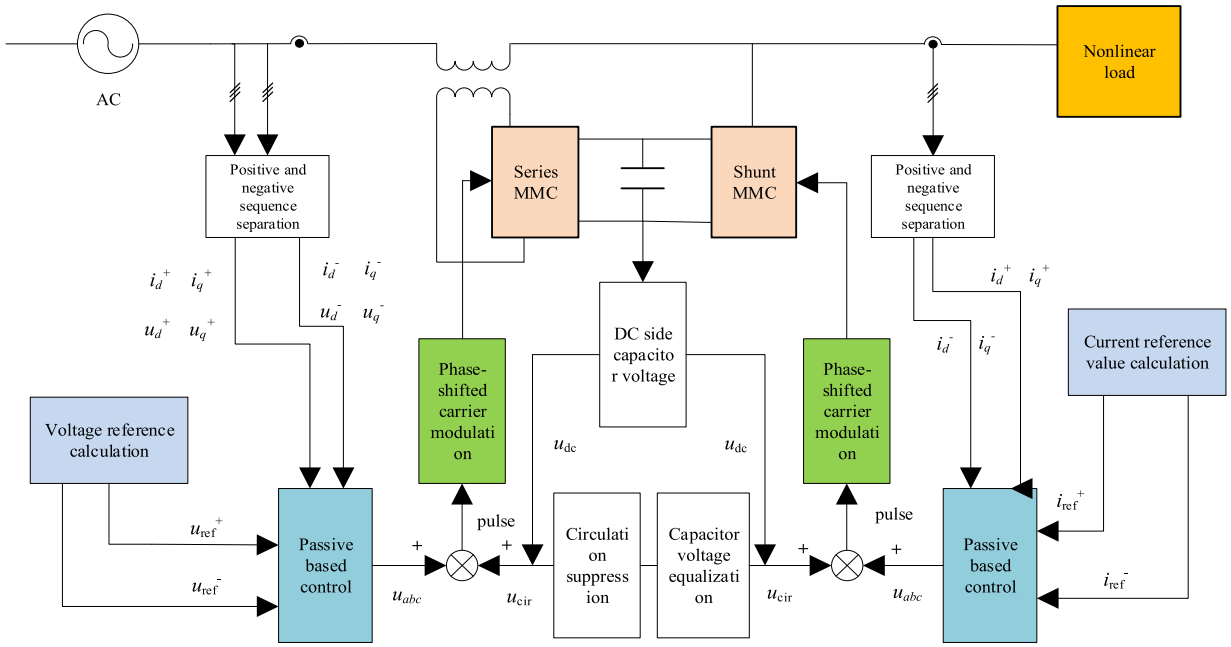

FIGURE 3. New control system structure of MMC-UPQC.

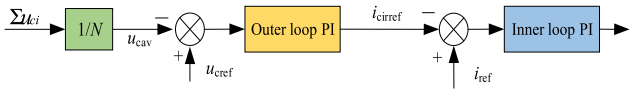

FIGURE 4. Block diagram of average capacitance voltage control.

controller and the equal voltage control output control quantity.

A. CAPACITANCE AVERAGE VOLTAGE CONTROL

Since MMC has 6 bridge arms and each arm contains N SMs, MMC has a huge number of SMs. Thus, the capacitive voltage stability of each SM affects the output waveform. Therefore, it is necessary to control the capacitance voltage does not to fluctuate. The average capacitance voltage control and the additional balance control are used to stabilize capacitance voltage of SMs.

The average capacitance voltage control is shown as Fig. 4. The voltage value of each SM is summed as Σ_{uci} and averaged as u_{cav}. The average voltage u_{cav} and average reference current $i$ref are controlled by PI to the set value.

The additional balance control is shown as Fig. 5. To ensure that the voltage u_{cna} of each SM is stable at the desired value, a proportional regulator Kp is used in control system. By setting the voltage reference value, the controller achieves the internal capacitance voltage balance. In Fig. 5, Δu_{jnaref} is each SM output control signal, where j represents the upper or lower bridge arms, and n ($n = 1, 2 \ldots N$) represents the individual SM of each bridge arm.

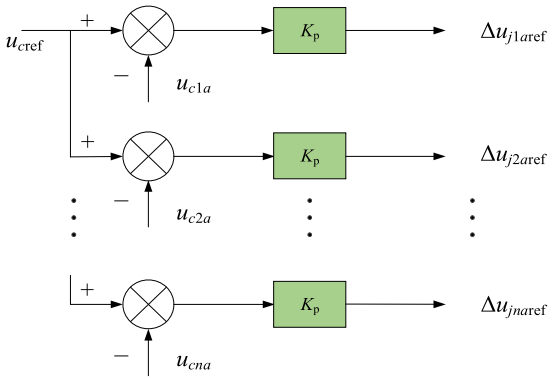

FIGURE 5. Block diagram of additional balance control for capacitance voltage.

B. CIRCULATING CURRENT SUPPRESSION CONTROL

When the grid is unbalanced, the circulating current of MMC becomes more severe. Taking a phase as an example, the circulating current contains not only the DC component, but also the alternating current (AC) component of 2 octave. In fact, the three-phase circulating current in the MMC flows in order of a-c-b, and the sum of the circulating currents of each phase is zero. From the mechanism of MMC's circulating current, the circulating current only exists inside the MMC.

The circulating current will not only affect the operation of power electronic devices, but also increase the system losses. In order to ensure the accuracy of the waveform, it is necessary to suppress circulating current. The circulating current is mainly composed of DC component and 2 octave component, in which 2 octave component is divided into positive sequence and negative sequence. There is no zero-sequence component of AC component because of the transformer of the line. The circulating current suppression control block diagram is shown as Fig. 6.

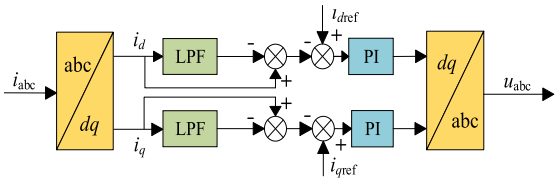

FIGURE 6. Block diagram of circulating current suppression control.

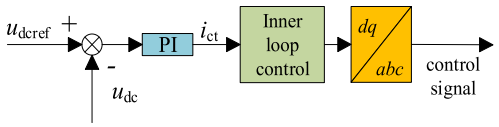

FIGURE 7. Block diagram of DC side capacitance voltage control.

The circulating current suppression method applied in this paper is as follows: the low-pass filter (LPF) is used to filter out the 2-multiplier component, and then the PI control method is used to control it to 0. The method can quickly eliminate the circulating current components of each bridge arm.

C. DC SIDE CAPACITOR VOLTAGE CONTROL

Since the MMCs on the series and shunt sides are connected through capacitor C_1 in the DC side, the stability of the DC side capacitance affects the capacitance voltage of the bridge arm and SMs, so it is essential to control the capacitance voltage of the DC side.

The control block diagram of the capacitance voltage controller is presented in Fig. 7. The control signal is combined with the compensation current obtained from the outer loop, then entering the inner loop.

The collected voltage signal is filtered and separated to the positive and negative sequence, then stabilized at the desired value by PI. As shown in Fig. 7, the command signal is obtained by adding i_{ct} to the compensation current signal of the MMC control outer loop. The signal then enters the inner loop to obtain the control signal. In this way, the capacitor voltage is controlled to ensure the stability of the DC side voltage. In Fig. 7, u_{dcref} is the reference value of the DC side capacitance voltage. i_{ct} represents the control amount after PI control.

IV. PSMC CONTROLLER DESIGN FOR MMC-UPQC

The Section IV introduces PBC and SMC theories, then combining the two control methods into PSMC. PBC is a control method that takes the structure characteristics of the object into account. By reconfiguring the energy of the system and injecting nonlinear damping, the system can achieve the desired control effect while satisfying the condition of global asymptotic stability. PBC makes full use of the physical structure of the system without compensating the "reactive force" part of the nonlinear term that does not affect the stability and simplifies the controller design. In addition, PBC system offers simple structure that is easy to implement. And PBC has global stability with no singularities. The E-L mathematical model of MMC-UPQC is established firstly. Then after the system of MMC-UPQC was proved to be strictly passive, the PBC is designed. SMC is then added to the MMC-UPQC control system to form the PSMC.

A. E-L MATHEMATICAL MODEL OF MMC-UPQC

By combining the series and shunt parts from (3) and (4), the model of MMC-UPQC in dq rotating frame can be obtained as

$$\begin{cases} u_{sd1} = u_{sd} + L\frac{\mathrm{d}i_d}{\mathrm{d}t} + R_{zid} - \omega L i_q \\ u_{sd1} = u_{sd} + L\frac{\mathrm{d}i_q}{\mathrm{d}t} + R_{zid} + \omega L i_d \end{cases} \tag{5}$$

where, u_{sq1} and u_{sd1} are the line voltages of s (s =r, p stands for MMCs on series side and shunt side) in the dq rotating frame, while u_{sq} and u_{sq} are output voltage of the MMC. L is the equivalent inductance. R_z and i_q represent the line resistance and the line current, respectively.

Since the E-L models of positive and negative sequence are symmetrical, only the model of positive sequence is used as an example to demonstrate the design process of the control method below.

The EL model is in the form given as

$$\dot{\boldsymbol{M}}\boldsymbol{x} + \boldsymbol{J}\boldsymbol{x} + \boldsymbol{R}\boldsymbol{x} = \boldsymbol{u} \tag{6}$$

of which,

$$\boldsymbol{M} = \begin{bmatrix} L & 0 \\ 0 & L \end{bmatrix}, \boldsymbol{J} = \begin{bmatrix} 0 & -\omega L \\ \omega L & 0 \end{bmatrix},$$
$$\boldsymbol{R} = \begin{bmatrix} R_z & 0 \\ 0 & R_z \end{bmatrix}, \boldsymbol{u} = \begin{bmatrix} u_{d1} - u_d \\ u_{d1} - u_q \end{bmatrix}$$

where, the positive and definite diagonal matrix $\boldsymbol{M}$ is formed by the energy storage element. $\boldsymbol{J}$ is the antisymmetric matrix of the positive and negative system. The symmetric positive definite matrix $\boldsymbol{R}$ can reflect the energy dissipation characteristic of the system. $\boldsymbol{x}$ is the state variable of the positive and negative system. $\boldsymbol{u}$ represents the input variable of the system.

The passivity of the system is proved as follows: The m-dimensional system is expressed as

$$\begin{cases} \dot{\boldsymbol{x}} = f(\boldsymbol{x}, \boldsymbol{u}) \\ \boldsymbol{y} = h(x) \end{cases} \qquad \boldsymbol{x}(0) = \boldsymbol{x}_0 \in \boldsymbol{R}^n \tag{7}$$

where, $\boldsymbol{x} \in \boldsymbol{R}^n$ is state variable. $\boldsymbol{u} \in \boldsymbol{R}^m$ is input variable. $\boldsymbol{y} \in \boldsymbol{R}^m$ is output variable, which is a function of $\boldsymbol{x}$ continuity. The function f $(\boldsymbol{x}, \boldsymbol{u})$ is local Lipschitz function.

For systems (7), if there is a continuous semi-positive definite energy storage function $\boldsymbol{H}(\boldsymbol{x})$ and a positive definite function $\boldsymbol{Q}(\boldsymbol{x})$, then the following inequalities hold.

$$\boldsymbol{H}(x(t)) - \boldsymbol{H}(x(0)) \le \int_0^t \boldsymbol{u}^T \boldsymbol{y} d\tau - \int_0^t \boldsymbol{Q}(x)\mathrm{d}t \tag{8}$$

or

$$\dot{\boldsymbol{H}}(\boldsymbol{x}) \le \boldsymbol{u}^T \boldsymbol{y} - Q(\boldsymbol{x}) \tag{9}$$

Generally, if the input $\boldsymbol{u}$, output $\boldsymbol{y}$ and energy supply rate of the system $\boldsymbol{uTy}$ holds, then the system is strictly passive. The energy storage function selected from (8) can be designed as

$$V = \boldsymbol{x}_{\mathrm{e}}^{\mathrm{T}}\boldsymbol{M}\boldsymbol{x}_{\mathrm{e}} = \boldsymbol{x}_{\mathrm{e}}^{\mathrm{T}}\left(\boldsymbol{u} - \boldsymbol{J}\boldsymbol{x}_{\mathrm{e}} - \boldsymbol{R}\boldsymbol{x}\mathrm{e}\right) = \boldsymbol{x}_{\mathrm{e}}^{\mathrm{T}}\boldsymbol{u} - \boldsymbol{x}_{\mathrm{e}}^{\mathrm{T}}\boldsymbol{R}\boldsymbol{x}_{\mathrm{e}}^{\mathrm{T}} \tag{10}$$

Let $\boldsymbol{y} = \boldsymbol{x}_{\mathrm{e}}^{T}, Q(\boldsymbol{x}) = \boldsymbol{x}_{\mathrm{e}}^{T}\boldsymbol{M}\boldsymbol{x}_{\mathrm{e}}$, and after simplification, the above conditions can be satisfied. Therefore, the MMC-UPQC system is strictly passive. According to the passive theory, we can prove that the MMC-UPQC system has stability. As a result, PBC is applicable to MMC-UPQC.

B. DESIGN OF SLIDER CONTROLLER BASED ON E-L MODULE

Under the *dq* coordinate system, the desired equilibrium point is determined. So, the PBC control strategy for MMC-UPQC can be designed. The equilibrium points of the system are given as

$$x^{+*} = \begin{bmatrix} i_{d\mathrm{ref}}^{+} \\ i_{q\mathrm{ref}}^{+} \end{bmatrix} x^{-*} = \begin{bmatrix} i_{d\mathrm{ref}}^{-} \\ i_{q\mathrm{ref}}^{-} \end{bmatrix} \tag{11}$$

where, $i_{d\mathrm{ref}}^{+}$, $i_{q\mathrm{ref}}^{+}$, $i_{d\mathrm{ref}}^{-}$, $i_{q\mathrm{ref}}^{-}$ denote the positive and negative order system in the state variables, and $i_d^{+}, i_q^{+}, i_d^{-}, i_q^{-}$ represent reference values.

The errors of the state variables for the system are expressed as

$$\begin{cases} \boldsymbol{x}_{\mathrm{e}}^{+} = \boldsymbol{x}^{+} - \boldsymbol{x}^{+*} \\ \boldsymbol{x}_{\mathrm{e}}^{-} = \boldsymbol{x}^{-} - \boldsymbol{x}^{-*} \end{cases} \tag{12}$$

The substitution of (12) is given as

$$\begin{cases} \boldsymbol{M}\boldsymbol{x}_{\mathrm{e}}^{+} + \boldsymbol{J}^{+}\boldsymbol{x}_{\mathrm{e}}^{+} + \boldsymbol{R}\boldsymbol{x}_{\mathrm{e}}^{+} = \boldsymbol{u}^{+} - \boldsymbol{M}\boldsymbol{x}^{+} - \boldsymbol{J}^{+}\boldsymbol{x}^{+*} - \boldsymbol{R}\boldsymbol{x}^{+*} \\ \boldsymbol{M}\boldsymbol{x}_{\mathrm{e}}^{-} + \boldsymbol{J}^{-}\boldsymbol{x}_{\mathrm{e}}^{-} + \boldsymbol{R}\boldsymbol{x}_{\mathrm{e}}^{-} = \boldsymbol{u}^{-} - \boldsymbol{M}\boldsymbol{x}^{-} - \boldsymbol{J}^{-}\boldsymbol{x}^{-*} - \boldsymbol{R}\boldsymbol{x}^{-*} \end{cases} \tag{13}$$

The error functions of the positive and negative order systems can be obtained as

$$V^{+} = \frac{\boldsymbol{x}_{\mathrm{e}}^{+\mathrm{T}}\boldsymbol{M}\boldsymbol{x}_{\mathrm{e}}^{+}}{2} \tag{14}$$

$$V^{-} = \frac{\boldsymbol{x}_{\mathrm{e}}^{-\mathrm{T}}\boldsymbol{M}\boldsymbol{x}_{\mathrm{e}}^{-}}{2} \tag{15}$$

From the above proof, it is known that the appropriate error function ensures that the system error energy function and the desired equilibrium point converge to 0, which indicates that the system is strictly passive. However, the size of the injection damping has a great influence on the convergence speed of the system. If the injection damping is too large or small, system convergence will slow down. Choosing proper injection damping can reduce oscillations, speed up convergence, and ensure the dynamic performance of the system. Therefore, the method of injection damping is adopted to accelerate the convergence of error function and improve its running speed.

The damping dissipation term is designed as

$$\begin{cases} \boldsymbol{R}_{\mathrm{h}}^{+}\boldsymbol{x}_{\mathrm{e}}^{+} = \left(\boldsymbol{R} + \boldsymbol{R}_{\mathrm{g}}^{+}\right)\boldsymbol{x}_{\mathrm{e}}^{+} \\ \boldsymbol{R}_{\mathrm{h}}^{-}\boldsymbol{x}_{\mathrm{e}}^{-} = \left(\boldsymbol{R} + \boldsymbol{R}_{\mathrm{g}}^{-}\right)\boldsymbol{x}_{\mathrm{e}}^{-} \end{cases} \tag{16}$$

where, $\boldsymbol{R}_{\mathrm{g}}^{+}$ and $\boldsymbol{R}_{\mathrm{g}}^{-}$ represent the damping matrix of positive and negative order. The damping matrix of new positive and negative order $\boldsymbol{R}_{\mathrm{h}}^{+}$ and $\boldsymbol{R}_{\mathrm{h}}^{-}$ can be expressed as:

$$\boldsymbol{R}_{\mathrm{g}}^{+} = \begin{bmatrix} R_{\mathrm{g1}}^{+} & 0 \\ 0 & R_{\mathrm{g2}}^{+} \end{bmatrix} \quad \boldsymbol{R}_{\mathrm{g}}^{-} = \begin{bmatrix} R_{\mathrm{g1}}^{-} & 0 \\ 0 & R_{\mathrm{g2}}^{-} \end{bmatrix} \tag{17}$$

where, $R_{\mathrm{g1}}^{+}, R_{\mathrm{g2}}^{+}, R_{\mathrm{g1}}^{-}, R_{\mathrm{g2}}^{-}$ are respectively the injected damping values of positive and negative sequences of d and q axes. In order to reduce the response time and speed up the operation of the system, it is necessary to use the injected damping matrix to increase the energy dissipation rate of the system. Then (13) becomes as (18), shown at the bottom of the page.

The following controller can be given as

$$\begin{cases} u_{sd}^{+} = u_d^{+} - R_{g1}^{+}\left(i_d^{+} - i_{d\mathrm{ref}}^{+}\right) + R_z i_{d\mathrm{ref}}^{+} - \omega L i_q^{+} \\ u_{sq}^{+} = u_q^{+} - R_{g2}^{+}\left(i_q^{+} - i_{q\mathrm{ref}}^{+}\right) + R_z i_{q\mathrm{ref}}^{+} - \omega L i_d^{+} \end{cases} \tag{19}$$

$$\begin{cases} u_{sd}^{-} = u_d^{-} - R_{g1}^{-}\left(i_d^{-} - i_{d\mathrm{ref}}^{-}\right) + R_z i_{d\mathrm{ref}}^{-} - \omega L i_q^{-} \\ u_{sq}^{-} = u_q^{-} - R_{g2}^{-}\left(i_q^{-} - i_{q\mathrm{ref}}^{-}\right) + R_z i_{q\mathrm{ref}}^{-} - \omega L i_d^{-} \end{cases} \tag{20}$$

where, u_{sd}^{+}, u_{sq}^{+}, u_{sd}^{-}, u_{sq}^{-} are voltage output voltage of MMC under positive and negative sequence in dq axis, $u_d^{+}, u_q^{+}, u_d^{-}$, u_q^{-} denote line voltages under positive sequence and negative sequence in dq axis respectively.

Under the condition of unbalanced grid voltage, the controller coefficients of PBC method for MMC-UPQC are fixed. When the load suddenly increases, the controller performs poor adaptability. Furthermore, PBC requires the model with precise parameters, but in practice the system parameters (such as system impedance) vary over time. Various uncertain factors in the running process of the device will have an impact on the operating balance point of the system, thus adversely affecting the performance of the controller. In other words, the parameters are difficult to be accurately controlled, resulting in slow reaction speed, poor compensation effect and poor adaptability especially in complex grid systems. However, SMC can resist the influence of external

$$\begin{cases} \boldsymbol{M}\boldsymbol{x}_{\mathrm{e}}^{+} + \boldsymbol{R}_{\mathrm{h}}^{+}\boldsymbol{x}_{\mathrm{e}}^{+} = \boldsymbol{u}^{+} - \left[\boldsymbol{M}\boldsymbol{x}^{+^*} + \boldsymbol{J}\left(\boldsymbol{x}^{+^*} + \boldsymbol{x}_{\mathrm{e}}^{+}\right) + \boldsymbol{R}\boldsymbol{x}^{+^*} - \boldsymbol{R}_{\mathrm{g}}^{+}\boldsymbol{x}_{\mathrm{e}}^{+}\right] \\ \boldsymbol{M}\boldsymbol{x}_{\mathrm{e}}^{-} + \boldsymbol{R}_{\mathrm{h}}^{-}\boldsymbol{x}_{\mathrm{e}}^{-} = \boldsymbol{u}^{-} - \left[\boldsymbol{M}\boldsymbol{x}^{-^*} + \boldsymbol{J}\left(\boldsymbol{x}^{-^*} + \boldsymbol{x}_{\mathrm{e}}^{-}\right) + \boldsymbol{R}\boldsymbol{x}^{-^*} - \boldsymbol{R}_{\mathrm{g}}^{-}\boldsymbol{x}_{\mathrm{e}}^{-}\right] \end{cases} \tag{18}$$

disturbance and internal parameters on the system. SMC has the characteristics of fast dynamic response and strong robustness. Therefore, we integrate the characteristics of the two control methods and design the PSMC controller in the current inner loop.

According to SMC theory, sliding mode surface $\boldsymbol{s}_1$ and $\boldsymbol{s}_2$ based on SMC can be expressed as

$$\begin{cases} \boldsymbol{s}_1 = \boldsymbol{x}^+ - \boldsymbol{x}^{+*} \\ \boldsymbol{s}_2 = \boldsymbol{x}^- - \boldsymbol{x}^{-*} \end{cases} \tag{21}$$

Then,

$$\begin{cases} \dot{I}_d &= -\frac{R_z}{L} i_d^+ + \omega i_q^+ + \frac{1}{L}\left(u_{sd}^+ - u_d^+\right) \\ \dot{I}_q &= -\frac{R_z}{L} i_q^+ + \omega i_d^+ + \frac{1}{L}\left(u_{sq}^+ - u_q^+\right) \end{cases} \tag{22}$$

where, $\dot{I}_d$ and $\dot{I}_q$ are the first derivatives of the positive sequence current in dq rotating frame. The main drawback of SMC is the chattering problem due to the discontinuous control. PSMC is prone to jitter during the sliding mode switching process. Here, the exponential approach law is used to eliminate jitter. In order to attenuate the jitter, the exponential method $\mathrm{sgn}(\boldsymbol{s}_1)$ and $\mathrm{sgn}(\boldsymbol{s}_2)$ are chosen. According to the approach rate of SMC, derivatives of $\boldsymbol{s}_1$ and $\boldsymbol{s}_2$ can be expressed as

$$\begin{cases} \dot{\boldsymbol{s}_1} = -\boldsymbol{\rho}^+ \mathrm{sgn}(\boldsymbol{s}_1) = -\frac{R_z}{L}\boldsymbol{x}^+ + \omega \boldsymbol{x}^+ + \frac{1}{L}\boldsymbol{u}^+ \\ \dot{\boldsymbol{s}_2} = -\boldsymbol{\rho}^- \mathrm{sgn}(\boldsymbol{s}_2) = -\frac{R_z}{L}\boldsymbol{x}^- + \omega \boldsymbol{x}^- + \frac{1}{L}\boldsymbol{u}^- \end{cases} \tag{23}$$

of which,

$$\boldsymbol{u}^+ = \begin{bmatrix} u_{sd}^+ - u_d^+ \\ u_{sq}^+ - u_q^+ \end{bmatrix}, \quad \boldsymbol{u}^- = \begin{bmatrix} u_{sd}^- - u_d^- \\ u_{sq}^- - u_q^- \end{bmatrix}$$
$$\boldsymbol{\rho}^+ = \begin{bmatrix} \rho_1 \\ \rho_2 \end{bmatrix}, \quad \boldsymbol{\rho}^- = \begin{bmatrix} \rho_3 \\ \rho_4 \end{bmatrix}$$

where, adjustment coefficients $\rho_1, \rho_2, \rho_3, \rho_4 > 0$.

To reduce the high-frequency jitter of SMC, the saturation function $\mathrm{sat}(\boldsymbol{s})$ is used instead of the symbolic function $\mathrm{sgn}(\boldsymbol{s})$ in the ideal sliding mode. Then, we can obtain as

$$\begin{cases} \dot{\boldsymbol{s}_1} &= -\boldsymbol{\rho}_1 \mathrm{sat}(\boldsymbol{s}_1) \\ \dot{\boldsymbol{s}_2} &= -\boldsymbol{\rho}_2 \mathrm{sat}(\boldsymbol{s}_2) \end{cases} \tag{24}$$

Thus, (23) can be rewritten as

$$\begin{cases} \boldsymbol{u}^+ &= -R_z \boldsymbol{x}^+ + \omega L \boldsymbol{x}^+ + \boldsymbol{\rho}_1 \mathrm{sat}(\boldsymbol{s}_1) \\ \boldsymbol{u}^- &= -R_z \boldsymbol{x}^- + \omega L \boldsymbol{x}^- + \boldsymbol{\rho}_2 \mathrm{sat}(\boldsymbol{s}_2) \end{cases} \tag{25}$$

According to the above formulas, we can design as

$$\begin{cases} i_{\mathrm{d}}^+ - i_{\mathrm{dref}}^+ &= \frac{\rho_1 sat(s_1)}{R_{\mathrm{g1}}^+ + R_z} \\ i_{\mathrm{q}}^+ - i_{\mathrm{qref}}^+ &= \frac{\rho_2 sat(s_1)}{R_{\mathrm{g2}}^+ + R_z} \end{cases} \tag{26}$$

So, the PSMC strategy is given as

$$\begin{cases} u_{\mathrm{d}}^+ &= u_{\mathrm{sd}}^+ + \omega L i_{\mathrm{q}}^+ - R_z i_{\mathrm{dref}}^+ + \frac{R_{\mathrm{g1}}^+ \rho_1 sat(s_1)}{R_{\mathrm{g1}}^+ + R_z} \\ u_{\mathrm{q}}^+ &= u_{\mathrm{sq}}^+ - \omega L i_{\mathrm{d}}^+ - R_z i_{\mathrm{qref}}^+ + \frac{R_{\mathrm{g2}}^+ \rho_2 sat(s_2)}{R_{\mathrm{g2}}^+ + R_z} \end{cases} \tag{27}$$

$$\begin{cases} u_{\mathrm{d}}^- &= u_{\mathrm{sd}}^- + \omega L i_{\mathrm{q}}^- - R_z i_{\mathrm{dref}}^- + \frac{R_{\mathrm{g1}}^- \rho_3 sat(s_3)}{R_{\mathrm{g1}}^- + R_z} \\ u_{\mathrm{q}}^- &= u_{\mathrm{sq}}^- - \omega L i_{\mathrm{q}}^- - R_z i_{\mathrm{qref}}^- + \frac{R_{\mathrm{g2}}^- \rho_4 sat(s_4)}{R_{\mathrm{g2}}^- + R_z} \end{cases} \tag{28}$$

$$\begin{cases} u_{sd}^+ &= u_d^+ - \frac{R_{\mathrm{g1}}^+ \rho_1 sat(s_1)}{R_{\mathrm{g1}}^+ + R_z} + R_z i_{d\mathrm{ref}}^+ - \omega L i_q^+ \\ u_{sq}^+ &= u_q^+ - \frac{R_{\mathrm{g2}}^+ \rho_2 sat(s_2)}{R_{\mathrm{g2}}^+ + R_z} + R_z i_{q\mathrm{ref}}^+ - \omega L i_d^+ \end{cases} \tag{29}$$

$$\begin{cases} u_{sd}^- &= u_d^- - \frac{R_{\mathrm{g1}}^- \rho_3 sat(s_3)}{R_{\mathrm{g1}}^- + R_z} + R_z i_{d\mathrm{ref}}^- - \omega L i_q^- \\ u_{sq}^- &= u_q^- - \frac{R_{\mathrm{g2}}^- \rho_4 sat(s_4)}{R_{\mathrm{g2}}^- + R_z} + R_z i_{q\mathrm{ref}}^- - \omega L i_d^- \end{cases} \tag{30}$$

C. STABILITY ANALYSIS OF PSMC

Since the positive and negative sequence structures of PSMC controller are symmetric, we use positive sequence as an example to prove the stability of controller. According to Lyapunov theory, the Lyapunov function is selected as

$$V(x) = \frac{1}{2} s_1^2 \tag{31}$$

where, $s_1 = x^+ - x^{+*}$, and x^{+*} is the positive order reference value of x. From (31), $V(x) = 0$ when $x = 0$. Since (31) includes the squared term of s_1, $V(x)$ is positive definite. Combining with (24), we can get

$$\dot{V}(x) = s_1 \dot{s}_1 = s_1(-\boldsymbol{\rho}_1 \mathrm{sat}(s_1)) \tag{32}$$

where,

$$\mathrm{sat}(s_1) = \begin{cases} 1 s_1 > \Delta \\ k_s\, s_1 \ |s_1| < \Delta \\ -1 s_1 < -\Delta \end{cases} \quad \Delta = \frac{1}{k_s} \tag{33}$$

where, k_s is a positive number. We discuss (32) for different cases as follows:

(1) When $s_1 > \Delta$, we have $\mathrm{sat}(s_1) = 1$, then (32) can be simplified as

$$\dot{V}(x) = s_1 \dot{s}_1 = -\boldsymbol{\rho}_1 s_1 \tag{34}$$

where $s_1 > 0$ and $\boldsymbol{\rho}_1 > 0$, so $\dot{V}(x)$ is negative definite.

(2) When $s_1 < -\Delta$, we have $\mathrm{sat}(s_1) = -1$, then (32) can be simplified as

$$\dot{V}(x) = s_1 \dot{s}_1 = \boldsymbol{\rho}_1 s_1 \tag{35}$$

where $s_1^{<0 and}$ $\boldsymbol{\rho}_1 > 0$, so $\dot{V}(x)$ is negative definite.

(3) When $|s_1| < \Delta$, we have sat $(s_1) = k_s s_1$, then (32) can be simplified as

$$\dot{V}(x) = s_1 \dot{s}_1 = -\boldsymbol{\rho}_1 k s_1^2 \tag{36}$$

where $\boldsymbol{\rho}_1 > 0$ and $k_s > 0$, so $\dot{V}(x)$ is negative definite. From the above proof, the PSMC has stability.

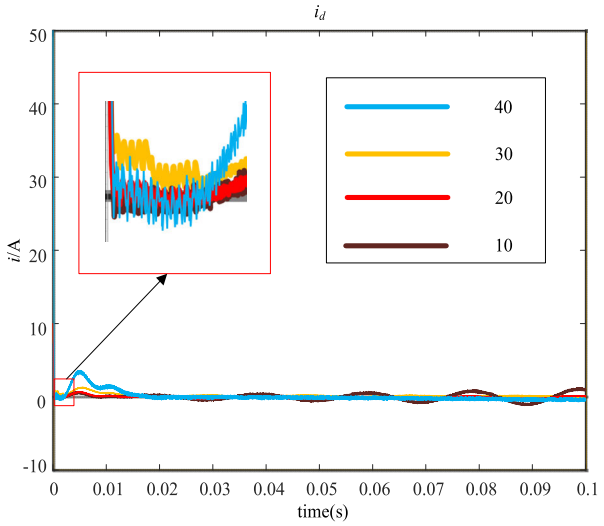

FIGURE 8. The waveforms of i_d under different adjustment coefficients.

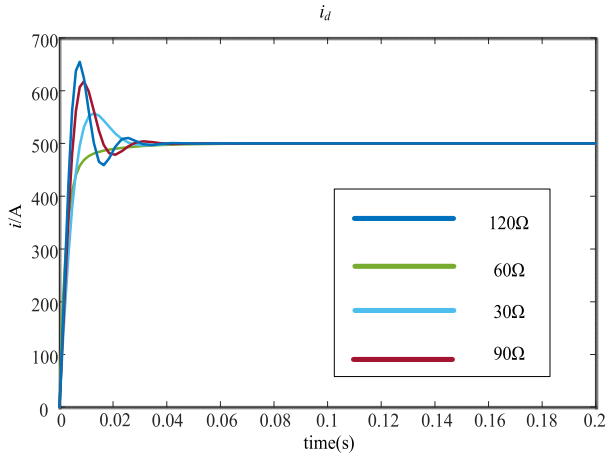

FIGURE 9. The waveforms of i_d under different damping coefficients.

D. SELECTION OF ADJUSTMENT COEFFICIENT FOR PSMC

Based on the derivation in the previous section, PSMC for MMC-UPQC contains four tuning parameters. Adjustment parameters have a great impact on the control effect of PSMC. So here, a tradeoff is considered for the design of control parameters. Considering the complexity and symmetry of the control system, ideally the four resistance adjustment parameters are selected to the same values. We find the appropriate parameters by observing the dynamic response and steady-state error of the grid current. In order to obtain better adjustment parameters and dynamic characteristics, the size of the adjustment parameter is adjusted, and grid current of the d-axis is observed as shown in Fig. 8.

As can be seen from Fig. 8, when $\rho = 40$, the overshoot is too large, which is not conducive to the operation of the controller. When $\rho = 10$, although the overshoot is small, it starts to be unstable and oscillates after 0.03s. When $\rho = 20$ or 30, the reaction speed is fast, and the output is stable. Since the overshoot at $\rho = 20$ is smaller than that at $\rho = 30$, the adjustment factor in this paper is equal to 20. In order to compare the control effects, the same adjustment parameters are chosen for PSMC and PBC.

E. SELECTION OF INJECTION DAMPING COEFFICIENT FOR PSMC

PSMC based on the EL model for MMC-UPQC also contains four injection damping parameters. When the model parameters are not accurate enough or the main circuit parameters are offset, the PBC strategy will show poor effect. So, accurate injection damping parameter is required in PSMC. Similarly, considering the complexity and symmetry of the control system, the four damping parameters are also chosen to have the same values. In order to obtain better damping parameters and dynamic characteristics, the size of the injected damping is regulated, and grid current of the d-axis is observed. The waveform is shown as Fig. 9.

In Fig. 9, when $R = 30\ \Omega$ and $R = 90\ \Omega$, the system has a large amount of overshoot and a long adjustment time. When $R = 60\ \Omega$, the performance and stability of the system will be much better compared with the cases of other resistance values. Therefore, the resistance value $R = 60\ \Omega$ is chosen.

F. BODE DIAGRAM ANALYSIS OF HARMONIC REJECTION CAPABILITY

Fig. 10 shows the Bode diagrams for the three different controllers are applied to MMC-UPQC at the fundamental frequency and the 3rd, 5th and 7th harmonic frequencies. Compared with PI and PBC, PSMC has advantages in harmonic rejection. Fig. 10(a) shows the Bode diagram for PSMC controller is applied. PSMC has the amplitude margin of 40 dB, 50 dB, 60 dB at the 3rd, 5th and 7th harmonic frequencies, respectively. Compared with PBC and PI, PSMC has a larger amplitude margin. And the phase angle margin is around 45 degrees as shown in Fig. 10(a). Therefore, PSMC is able to compensate these harmonics. In addition, the PSMC controller does not interfere with each other at the resonant frequency of each specified harmonic, which ensures that PSMC for MMC-UPQC can better compensate the harmonic voltage and current to improve the power quality. Fig. 10(a) shows that PSMC can effectively manage and suppress harmonics.

Fig. 10(b) shows the Bode diagram for the PBC controller is applied. In Fig. 10(b), PBC controller has a weak attenuation effect on harmonics. As shown in Fig. 10(b), the amplitude of the PBC is 5 dB at the 3rd harmonic and is smaller at the 5th and 7th harmonics, which indicates that the PBC is less effective in compensating these harmonics as compared with PSMC.

Fig. 10(c) shows the Bode diagram for the PI controller is applied. The PI control also has poor amplitude and frequency characteristics at harmonic frequencies as shown in Fig. 10(c). The gain of PI at the 3rd harmonic frequency is about 1 dB. After 150 Hz, the phase angle margin of PI decreases as the frequency increases. So, the suppression of

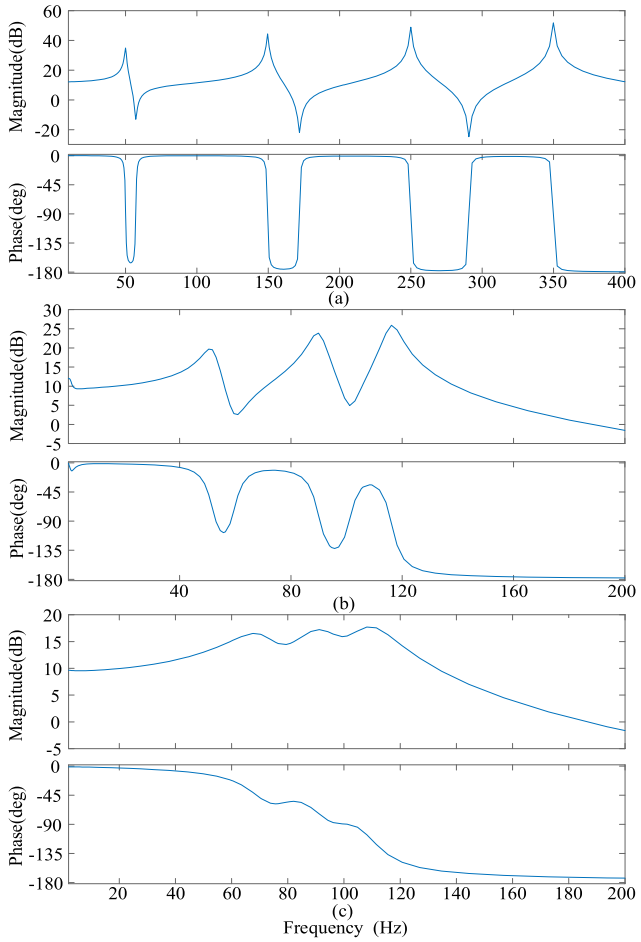

FIGURE 10. The Bode diagrams for the three different controllers are applied to MMC-UPQC at the fundamental frequency and the 3rd, 5th and 7th harmonic frequencies. (a) The Bode diagram for PSMC controller is applied. (b) The Bode diagram for PBC controller is applied. (c) The Bode diagram for PI controller is applied.

these harmonics by PI control is limited. And the margin of PI changes little when the frequency changes. Fig. 10(c) shows that the PI is difficult to recover harmonics at the 3rd, 5th and 7th frequencies.

V. SIMULATION RESULTS

In order to verify the effectiveness of the proposed control strategy, PSMC for MMC-UPQC has been simulated using MATLAB/Simulink. The simulation parameters used in the simulation are given in Table 1. Since PSMC is a control method derived from PBC and PI control has matured in industry, we compare the control effect of PSMC with PBC and PI. By comparing with PBC and PI control, the superiority of PSMC is verified by simulation. As a result, PMSC can better adapt to the changes in the power systems and output a more stable waveform. The following Fig. 11 shows the output waveform of PBC and PSMC during the sudden change on the load side.

As can be seen from the Fig. 11(b) that when the load suddenly increases, the PBC controller is poorly adaptable

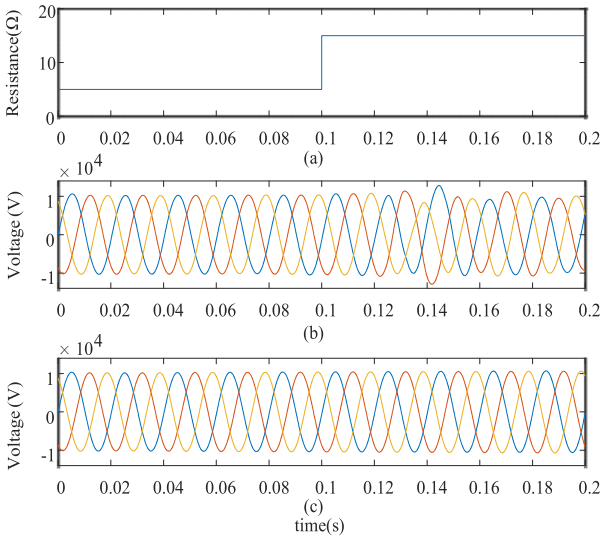

FIGURE 11. Comparison of PSMC and PBC for adaptation of system parameters. (a) System parameter changes. (b) Response of PBC. (c) Response of PSMC.

TABLE 1. Simulation parameters.

System parameters	Parameter value
Number of bridge arm modules N	8
AC voltage/kV	10
DC side capacitance voltage/kV	2.1
DC side capacitance/mF	10
Transformer ratio	10/2.1
Bridge capacitance/mF	0.1
Bridge arm inductance/mH	13
Sub-module capacitance voltage/kV	0.6
Sub-module capacitance/mF	0.47
Bridge capacitance/mF	0.047
Bridge arm inductance/mH	2
Load Resistance/Ω	5
Damping Coefficient/Ω	60
Adjustment Coefficient	20

because the controller coefficients are fixed. What is more, PBC does not stabilize quickly after a sudden change in parameters. Compared with the PBC, PSMC is less affected by the system parameters.

Fig. 12 shows the simulation of the circulating currents for the three controllers are applied. Compared with PBC and PI, the circulating current for PSMC control is small and stable as shown in Fig. 12. The circulating current for PI control is about 400 A, and can be lowered to 150 A under PBC. Compared with PBC and PI, PSMC can suppress the circulating current within 20 A as shown in Fig. 12(c). As shown in the Fig. 12, transition time of PSMC is as small as 0.005 s. In addition, the response speed of PSMC is the

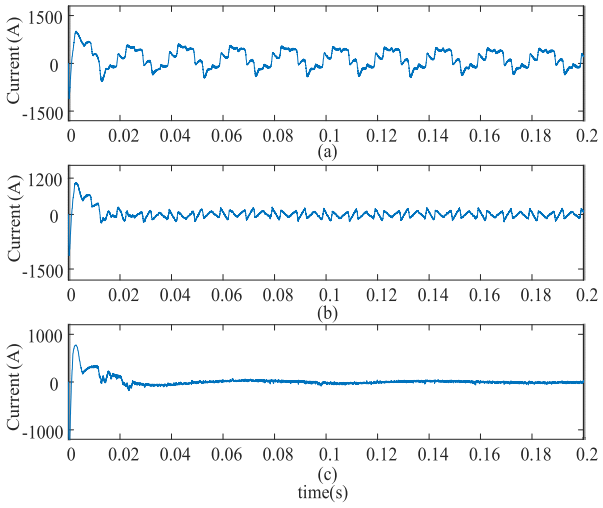

FIGURE 12. The simulation of the circulating currents for the three controllers are applied to MMC-UPQC. (a) Circulating current for PI. (b) Circulating current for PBC. (c) Circulating current for PSMC.

TABLE 2. Comparison of three control methods for MMC on series side under the temporary voltage swell.

Indicator (unit)	PI	PBC	PSMC
Recovery time (s)	0.05	0.02	0.005
Overshoot (%)	3.2	1.2	0.3
Total harmonic distortion (%)	8.62	4.37	0.86

TABLE 3. Comparison of three control methods for MMC on series side under the temporary voltage sag.

Indicator (unit)	PI	PBC	PSMC
Recovery time (s)	0.02	0.01	0.003
Overshoot (%)	1.5	1.0	0.2
Total harmonic distortion (%)	5.24	3.96	0.46

fastest and the response time of PSMC control is the shortest as shown in Fig. 12(c).

A. VOLTAGE COMPENSATION SIMULATION OF MMC IN SERIES

In this case, the a-phase voltage has a temporary swell of 20% from 0.02 s to 0.08 s. In addition, the 20% transient sag occurs from 0.12 s to 0.18 s, causing the power grid voltage unbalanced. Under this disequilibrium condition, the comparative simulation results from the three control methods are shown as Fig. 13 and Table 2 and Table 3.

As can be seen from Fig. 13 when the voltage sags or swells, the voltage fluctuation of PSMC is smaller than that of the other two control methods. PSMC achieves the control goal within 0.005 s, whereas PI and PBC need at least 0.05 s as shown in Figs. 13(e) and 13(g), which indicates that the

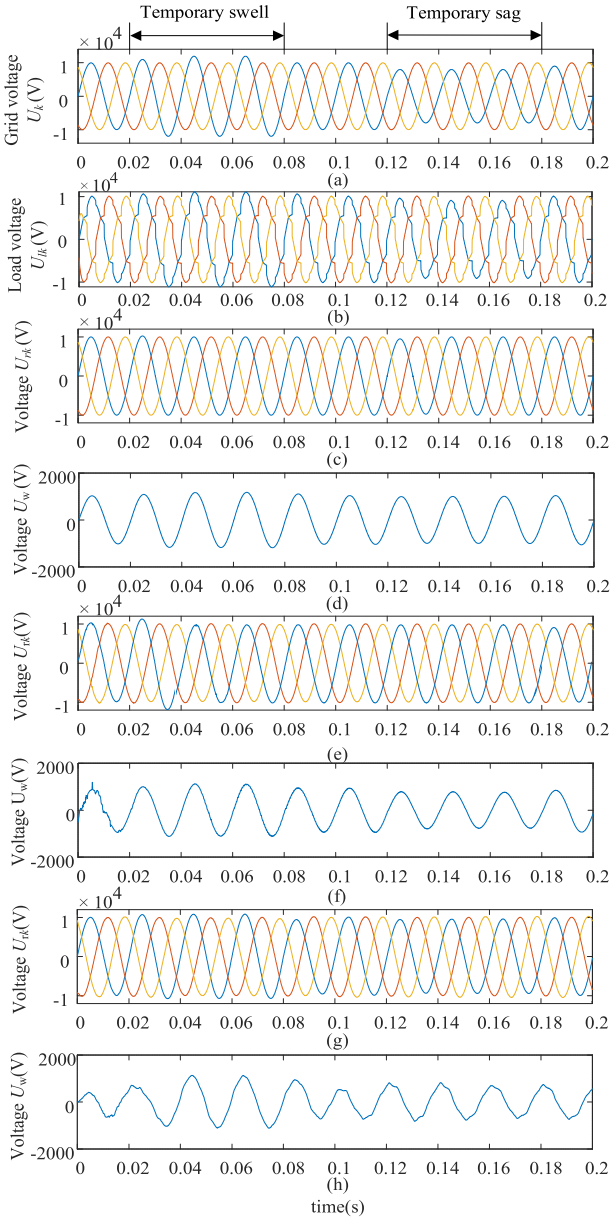

FIGURE 13. Comparison of three voltage compensation methods for MMC on series side under unbalanced grid voltage. (a) Grid voltage. (b) Load voltage. (c) Load-side voltage under the proposed PSMC. (d) Compensation voltage under PSMC. (e) Load-side voltage under PBC. (f) Compensation voltage under PBC. (g) Load-side voltage under PI. (h) Compensation voltage under PI.

PSMC reaches the balance in a shorter time than PI control. The total harmonic distortion degree (THD) of voltage is 0.86% after the restoration from PSMC. As shown in the Table 2, harmonic component under PSMC is smaller those under PI and PBC. Therefore, the PSMC for the MMC on series side can compensate the voltage quickly and accurately. The PSMC has better compensation performance, and its voltage compensation is fast and stable.

In order to reflect the ability to handle grid voltage harmonics, the 3rd harmonic with amplitude 2500 V is injected at 0.05 s, thus causing the total harmonic distortion is large

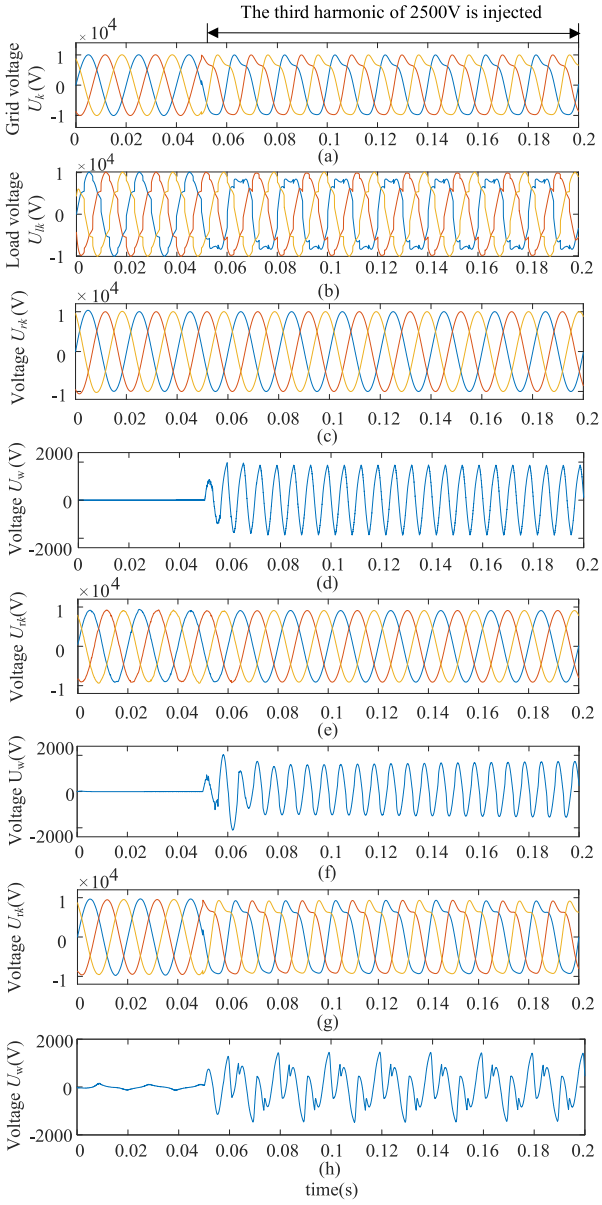

FIGURE 14. Comparison of three voltage compensation methods for MMC on series side when the grid voltage is injected with harmonics. (a) Grid voltage. (b) Load voltage. (c) Load-side voltage under the proposed PSMC. (d) Compensation voltage under PSMC. (e) Load-side voltage under PBC. (f) Compensation voltage under PBC. (g) Load-side voltage under PI. (h) Compensation voltage under PI.

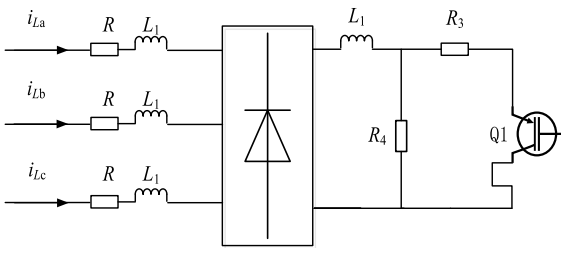

FIGURE 15. Nonlinear load circuit of MMC on shunt side.

(THD=32%). The simulation results are shown as Fig. 14 and Table 4.

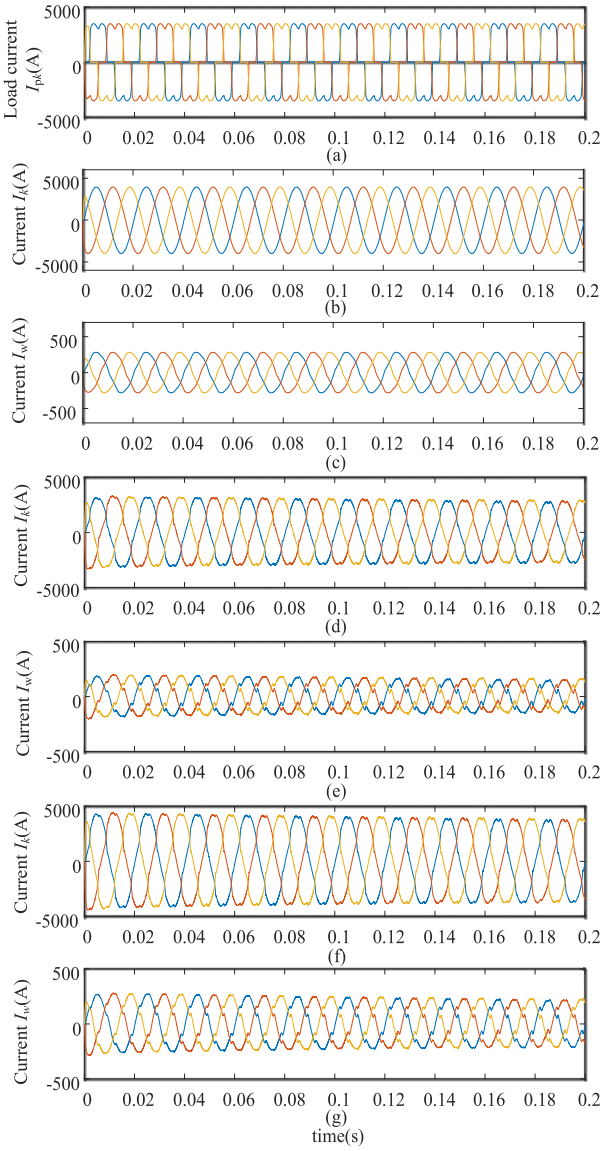

FIGURE 16. Comparison of three current compensation methods for MMC on shunt side under nonlinear load. (a) Load current. (b) Grid current under PSMC. (c) Compensation current under PSMC. (d) Grid current under PBC. (e) Compensation current under PBC. (f) Grid current under PI. (g) Compensation current under PI.

As can be seen from Fig. 14, the compensation effect of PSMC is much better than PI and PBC. When simulation time reaches 0.005 s, the control target of PSMC can be achieved with THD of 0.95%, whereas the PI control only reduces the degree of harmonic distortion and cannot compensate harmonics well with THD of 7.53%. In addition, from the perspective of the compensation waveform, PSMC has been stable within 0.05 s, but the PI control has been fluctuating as shown in Fig. 14(h). So, PSMC is faster and more stable than PI control to compensate harmonics.

B. CURRENT COMPENSATION SIMULATION OF MMC IN SHUNT

In this paper, the nonlinear load of the shunt side uses a resistor R_3 and an IGBT in series with the

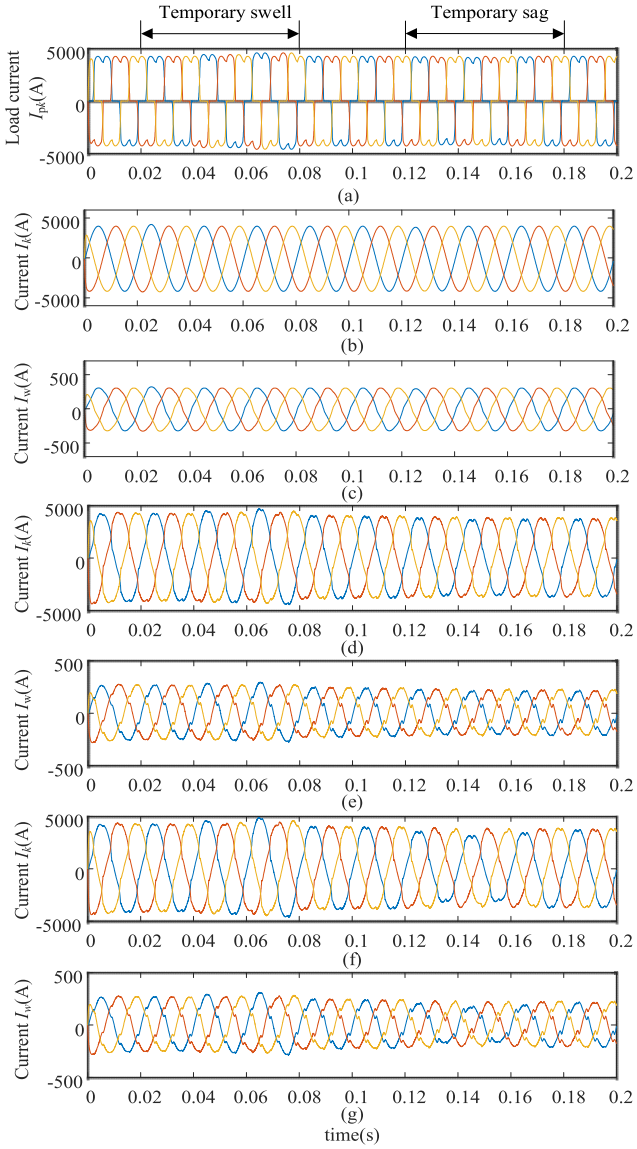

FIGURE 17. Comparison of three current compensation methods for MMC on shunt side under unbalanced grid voltage. (a) Load current. (b) Grid current under PSMC. (c) Compensation current under PSMC. (d) Grid current under PBC. (e) Compensation current under PBC. (f) Grid current under PI. (g) Compensation current under PI.

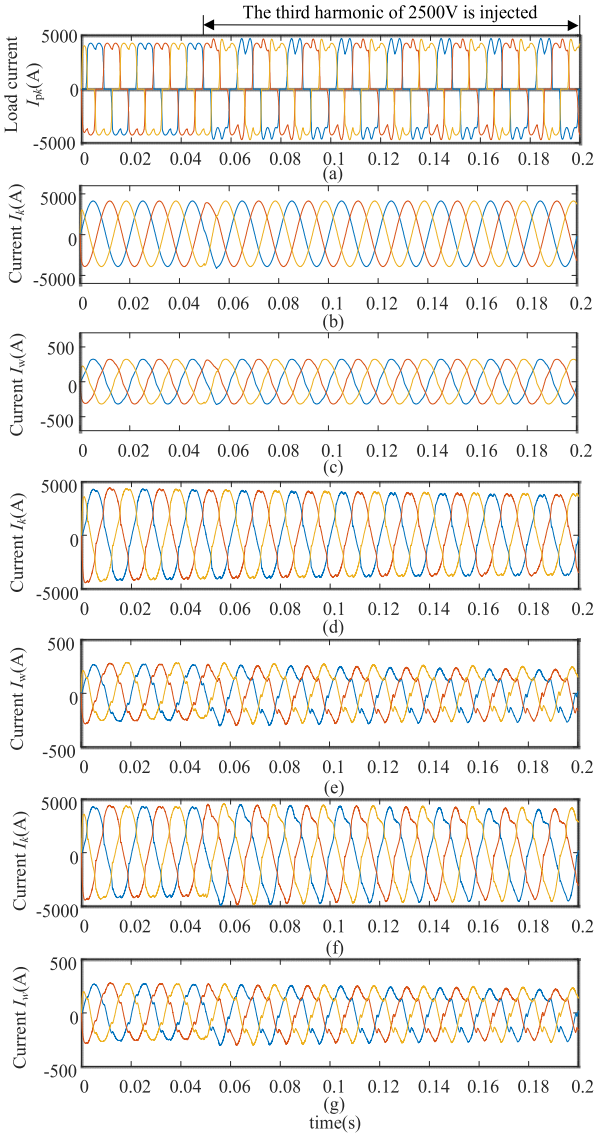

FIGURE 18. Comparison of three current compensation methods for MMC on shunt side when the load current is injected with harmonics. (a) Load current. (b) Grid current under PSMC. (c) Compensation current under PSMC. (d) Grid current under PBC. (e) Compensation current under PBC. (f) Grid current under PI. (g) Compensation current under PI.

resistive load through the RL buffer circuit, as shown in Fig. 15.

When nonlinear load exists at the load side, the current contains many harmonics. The harmonic distortion degree is large with THD of 23.7%. The simulation results are shown as Fig. 16 and Table 5.

As can be seen from the Fig. 16, after 0.008 s the grid current becomes stable under PSMC, whereas the grid current under PBC is fluctuating until 0.06 s. Besides, the waves in PI control fluctuates greatly, but PSMC can restore the grid current to sine in Fig. 16(b). Both PSMC and PI control can compensate current harmonics, but THD of 1.46% under PSMC is smaller than that of 5.74% under PI control as shown in Table 5. Therefore, when the shunt MMC adopts PSMC, the compensating recovery speed and effect for current are significant.

When the power grid voltage swells and sags temporarily, the load current will be greatly affected. Thus, it is very important to recover the harmonic current in the case of temporary swell and sag. The simulation results of MMC on shunt side for voltage swell and sag are shown in Fig.17 and Table 6 and Table 7.

It is apparent from the Fig.17 that the current under PSMC control reaches stability at 0.004 s during the transient swell and 0.007 s during the transient sag. While the PI control requires 0.04 s to achieve the current stability. The PI control has large fluctuations and large overshoot as shown in Fig. 17(f). And we can get THD of 0.76% under PSMC

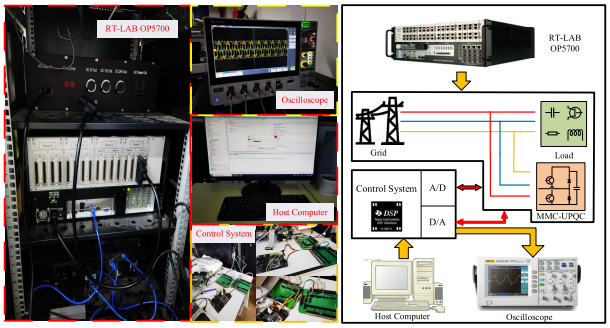

FIGURE 19. RT-LAB HIL test setup.

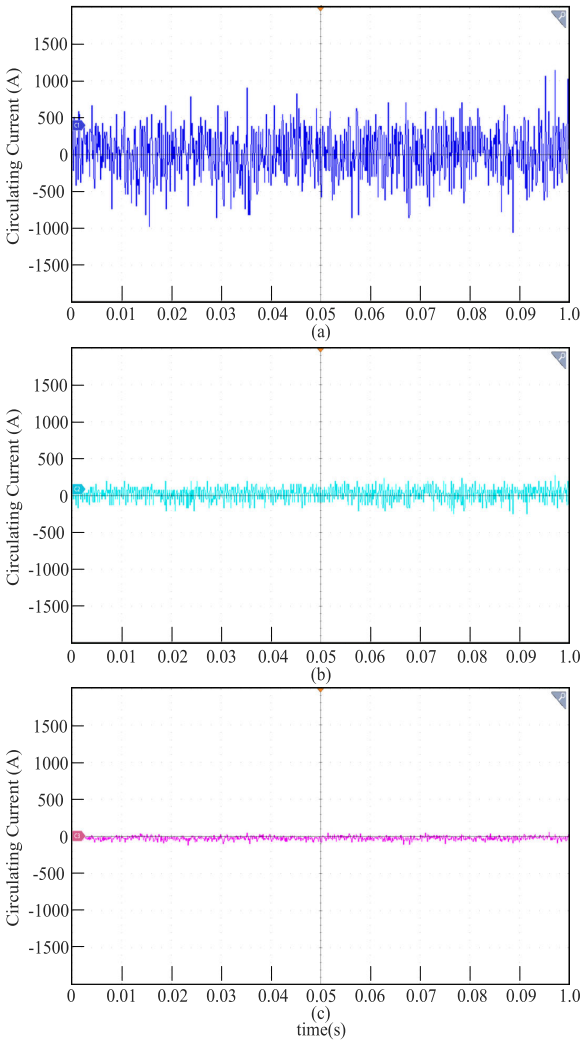

FIGURE 20. The circulating current for the three controllers on the RT-LAB experimental platform. (a) Circulating current for PI. (b) Circulating current for PBC. (c) Circulating current for PSMC.

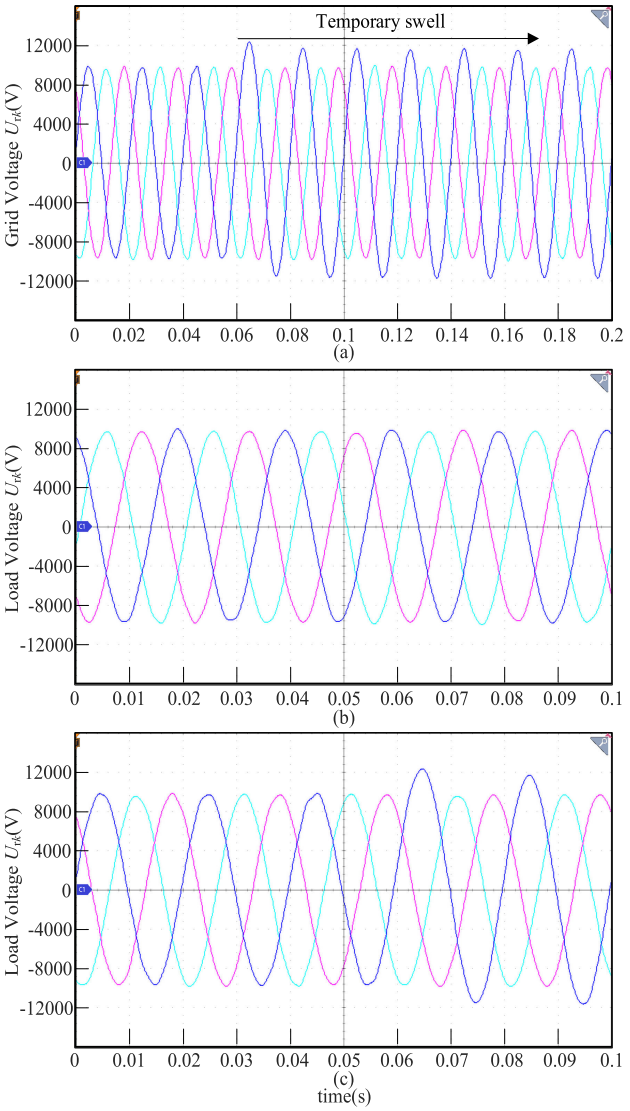

FIGURE 21. HIL test results of MMC on series side under unbalanced grid voltage. (a) Grid voltage. (b) Load-side voltage under the proposed PSMC. (c) Load-side voltage under PI.

TABLE 4. Comparison of three control methods for MMC on series side when series voltage is injected into harmonic.

Indicator (unit)	PI	PBC	PSMC
Recovery time (s)	0.09	0.015	0.005
Overshoot (%)	5.8	1.3	0.8
Total harmonic distortion (%)	7.53	6.35	0.95

and THD of 3.96% under PBC in Table 5. So, PSMC has shorter transition time, more stable output waveform, and better current compensation effect.

In order to demonstrate the ability to handle grid voltage harmonics, the 3rd harmonic with amplitude 2500 V is injected at 0.05 s, thus causing the total harmonic distortion is large (THD=32%). The simulation results are shown as Fig. 18 and Table 8.

As shown in Fig. 18, the current is compensated at 0.003 s using PSMC, while the PI control cannot completely compensate the harmonic amount. Compared with PSMC, the compensation effect under PBC is not good as shown in Fig. 18(d). The PSMC takes only 0.005 s to restore the grid current to a sinusoidal waveform. Therefore, PSMC has

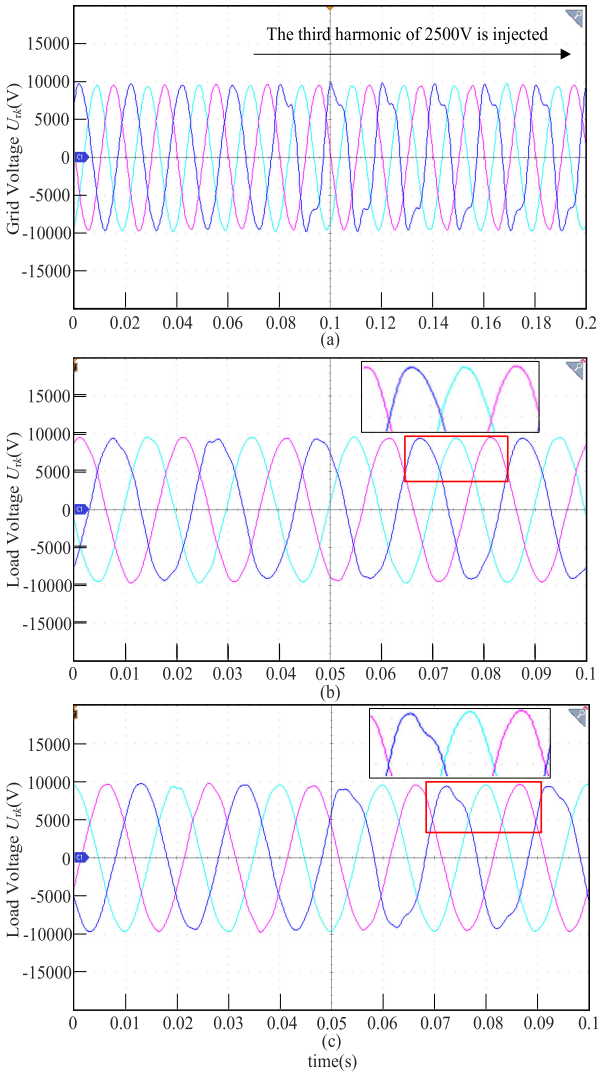

FIGURE 22. HIL test results of MMC on series side when the grid voltage is injected with harmonics. (a) Grid voltage. (b) Load-side voltage under the proposed PSMC. (c) Load-side voltage under PI.

TABLE 5. Comparison of three control methods for MMC on shunt side under nonlinear load.

Indicator (unit)	PI	PBC	PSMC
Recovery time (s)	0.06	0.018	0.008
Overshoot (%)	14	9.4	2.3
Total harmonic distortion (%)	5.74	2.76	1.46

better suppression of harmonics when harmonic interference occurs.

VI. EXPERIMENTAL VALIDATION

To further verify the feasibility of the PSMC strategy, the RT-LAB based HIL experimental platform is set up, as shown in Fig. 19. The RT-LAB OP5700 is used to simulate the MMC-UPQC system. The PSMC controller is implemented

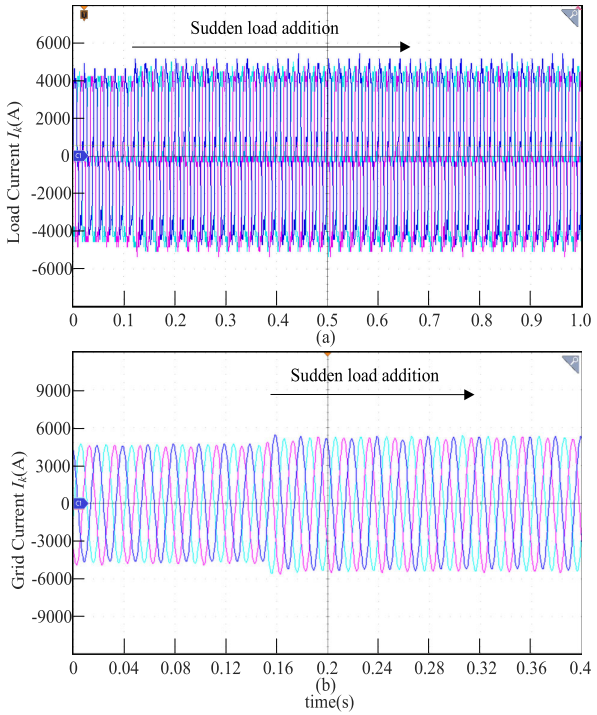

FIGURE 23. HIL test results of MMC on shunt side when the load suddenly increases. (a) Load current. (b) Grid current under PSMC.

TABLE 6. Comparison of three control methods for MMC on shunt side under the temporary voltage swell.

Indicator (unit)	PI	PBC	PSMC
Recovery time (s)	0.04	0.03	0.004
Overshoot (%)	4.3	3.2	1.2
Total harmonic distortion (%)	8.62	4.37	0.86

by using the Digital Signal Processor (DSP) Texas Instrument TMS320F28335 Board. The oscilloscope Tektronix MDO34 and host computers are used to observe the output waveform and the device operation. The experimental parameters are the same as in the simulations.

Fig. 20 shows the circulating currents for the three controllers on the RT-LAB experimental platform. As shown in Fig. 20, there is a significant difference in the amplitude of the circulating current under the three controllers. In Fig. 20, the circulating current is the smallest under the PSMC. Compared with PSMC, the current fluctuates more sharply under PBC and PI as shown in Fig. 20. Therefore, PSMC can eliminate the circulating current flow better, which ensures that MMC-UPQC can operate more stably.

A. VOLTAGE COMPENSATION EXPERIMENT OF MMC IN SERIES

The experiments of MMC on series side were carried out in the voltage swell and harmonic injection states. The experimental results are shown in Figs. 21 and 22, respectively.

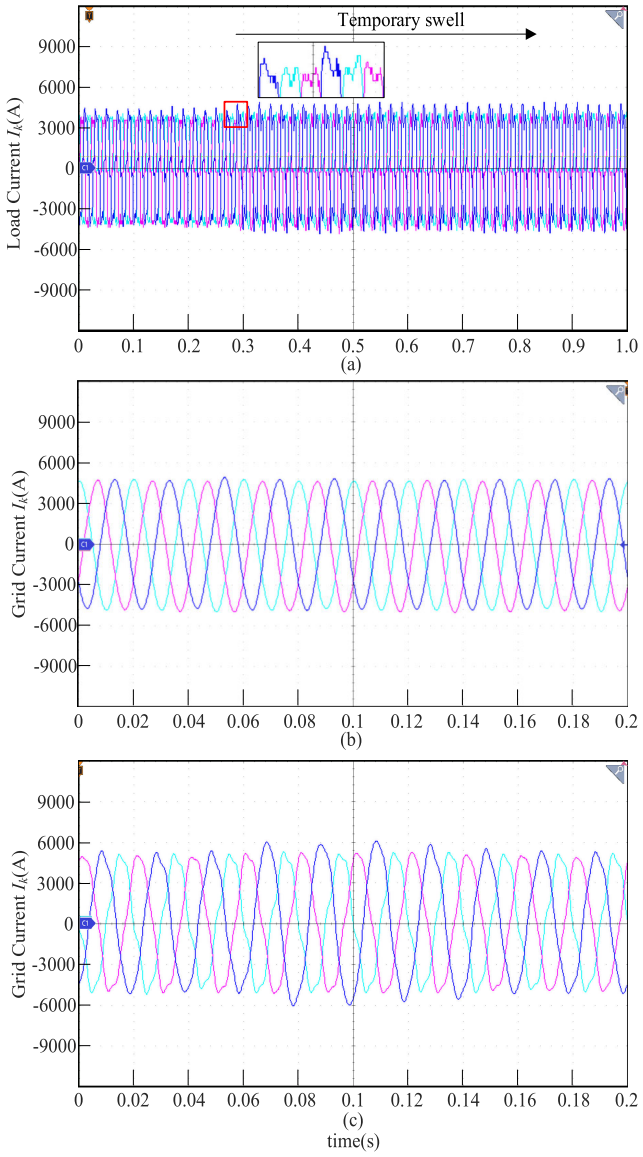

FIGURE 24. HIL test results of MMC on shunt side under unbalanced grid voltage. (a) Load current. (b) Grid current under PSMC. (c) Grid current under PI.

Fig. 21 shows the recovery of the load voltage under PSMC in the case of temporary swell. In the experiment, the grid voltage temporarily swells by 20% at 0.06 s. PSMC can restore the unbalance caused by the grid voltage swell in a single phase within 0.003 s as shown in Fig. 21. When PI is adopted, the waveform does not recover quickly to the set value. The flattened waveform after recovery shows the PSMC is helpful to improve voltage quality.

As shown in Fig. 22, the third harmonic of 2500 V is injected in grid voltage. In Fig. 22, it is easier to observe the control effect of PSMC and PI by enlarging the red box section. The THD of load voltage can be reduced from 32% to 1.23% after adopting PSMC for MMC-UPQC. Compared with THD of 4.62% after PI control, PSMC waveform contains less harmonics and has better control effect.

TABLE 7. Comparison of three control methods for MMC on shunt side under the temporary voltage sag.

Indicator (unit)	PI	PBC	PSMC
Recovery time (s)	0.04	0.015	0.007
Overshoot (%)	5.5	1.5	1.0
Total harmonic distortion (%)	5.24	3.96	0.76

TABLE 8. Comparison of three control methods for MMC on shunt side under when the load is injected with harmonics.

Indicator (unit)	PI	PBC	PSMC
Recovery time (s)	0.06	0.018	0.003
Overshoot (%)	14	9.4	6.3
Total harmonic distortion (%)	5.74	2.76	1.35

B. CURRENT COMPENSATION EXPERIMENT OF MMC IN SHUNT

The current recovery effect of MMC on shunt side will be verified under three cases: load switching, temporary swell and harmonic injection. The experimental results are shown in Figs 23, 24 and 25.

In that case, due to the sudden connection of another nonlinear load at the load side, the grid current also changes consequently. When the PSMC is adopted, the grid current can be restored to a sine wave as shown in Fig. 23. The grid current under PSMC control remains stable with THD of 2.69% even after load switching. Therefore, PSMC has a good ability to compensate current harmonics.

Fig. 24 shows the compensation of the PSMC and PI for grid currents when voltage swell. PSMC reacts quickly and restores the temporary swell in grid current within 0.005 s, which is similar to the simulation results. For PI control, an eight percent overshoot exists after control stabilization. As can be seen from Fig. 24, the control effect of PSMC is better than PI control, with shorter response time and smoother waveform.

To further verify the performance of the PSMC, the third harmonic of 2500 V was injected simultaneously under a nonlinear load as shown in Fig. 25. When taking PSMC, THD of grid current can be reduced from 35% to 1.56%. PSMC takes only 8 ms for grid current to reach a steady state. When PI is used, there are still some harmonics that are not offset with THD of 6.12%, resulting in incomplete recovery. Therefore, PSMC has a strong ability to compensate harmonics and can restore the grid current accurately.

C. THE ANALYSIS OF COMPUTATIONAL BURDEN

The operational status of the three control methods is shown in Table 9. First, the running time of MATLAB/Simulink is shown in Table 9. For a simulation time step of 0.2 s, the PI, PBC and PSMC takes time of 34.34 s, 35.32 s and 35.63 s,

TABLE 9. Comparison of the operational status of the three control methods.

Indicator (unit)	PSMC	PBC	PI
Simulation time (s)	35.63	35.32	34.34
Running space (bytes)	180,370	180,353	180,340
CPU usage (%)	29.49	29.06	22.67

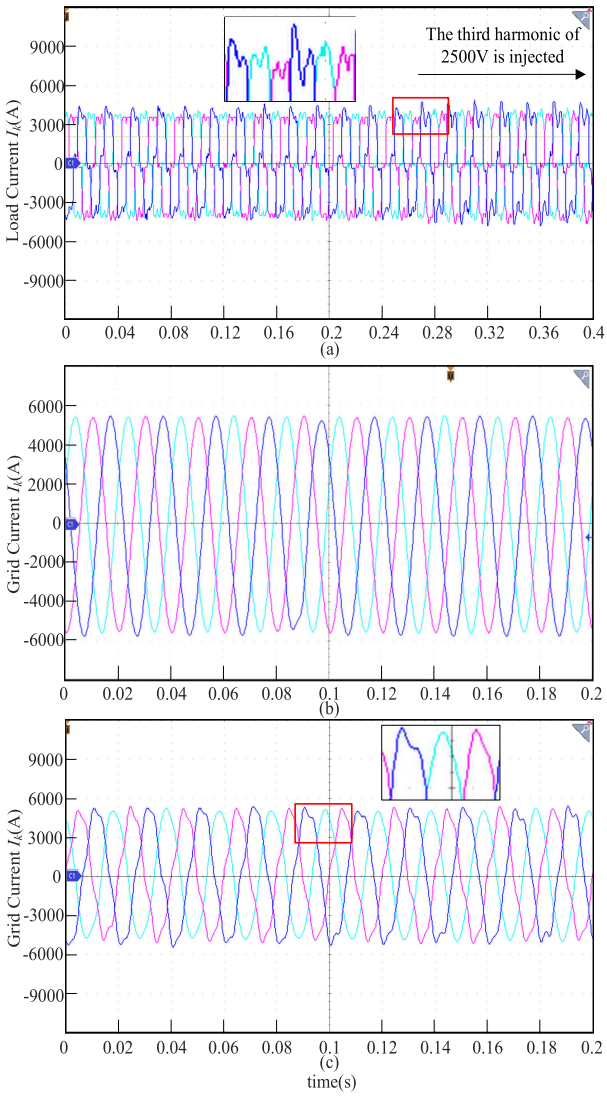

FIGURE 25. HIL test results of MMC on shunt side when the load current is injected with harmonics. (a) Load current. (b) Grid current under PSMC. (c) Grid current under PI.

respectively. So, PSMC will not increase the running time too much.

Second, the CPU usages of the three control methods are shown in Table 9. The usages are 22.67% under PI, 29.06% under PBC and 29.49% under PSMC, respectively. Therefore, PSMC does not occupy too much CPU memory compared with PI and PBC.

Finally, the PSMC, PBC and PI requires running space of 180,370 bytes, 180,353 bytes and 180,340 bytes, respectively. Compared with PBC control, PSMC is only 17 bytes more. According to the operational observation module of RT-LAB, model building and algorithm implementation of the three control methods are all in real time with no delays or timeouts, which means that the computational burden is within the tolerance of the experimental platform.

VII. CONCLUSION

This paper presents a PSMC strategy for MMC-UPQC system under grid unbalance. After the positive and negative sequence are separated, the PSMC strategy is used in current inner loop control. Combining with the circulating current suppression control method and the capacitor voltage control method, the PSMC can better restore power quality. The control performance improvement of PSMC enables stable device operation and improved economics. Simulation and HIL test results show that:

(1) PSMC has better control effect compared with PI control. The output waveform has fluctuation and the compensation effect is poor under PI control. Compared with the PI control, the proposed PSMC has the characteristics of shorter response time, stronger stability and better control effect. PSMC can recover voltage and current quality within 0.05 s, reducing harmonic distortion to less than 5%.

(2) Compared with PBC, the proposed PSMC has a better ability of adapting to complex system changes. As a result, PSMC is more stable and effective when the system structure or parameters are changed. Under grid voltage unbalance conditions, PSMC can quickly respond and restore voltage and current.

(3) Compared with PBC and PI, the overshoot is smaller and the recovered waveform is closer to sine wave under PSMC. The PSMC for MMC-UPQC can effectively solve the harmonic, unbalance, current imbalance and nonlinear problems. The simulation and HIL test results prove the effectiveness and superiority of the proposed PSMC system for power quality compensation.

REFERENCES

[1] H. Pang, D. Liu, L. Kou, H. Gu, and Z. Mi, "Design method of laboratory-scale MMC physical simulation system considering multiharmonic simulation accuracy," *IEEE J. Emerg. Sel. Topics Power Electron.*, vol. 10, no. 1, pp. 1017–1031, Feb. 2022.

[2] Y. Zhong, N. Roscoe, D. Holliday, T. C. Lim, and S. J. Finney, "High-efficiency MOSFET-based MMC design for LVDC distribution systems," *IEEE Trans. Ind. Appl.*, vol. 54, no. 1, pp. 321–334, Aug. 2017.

[3] J. Kang, D.-W. Kang, J.-P. Lee, D. W. Yoo, and J. W. Shim, "Design procedure of MMC-HVDC system: Comprehensive consideration of internal and external dynamics," *IEEE Access*, vol. 8, pp. 157437–157450, 2020.

[4] A. Ghosh and G. Ledwich, "A unified power quality conditioner (UPQC) for simultaneous voltage and current compensation," *Electr. Power Syst. Res.*, vol. 59, no. 1, pp. 55–63, Aug. 2001.

[5] A. M. Shotorbani, X. Meng, L. Wang, and B. Mohammadi-Ivatloo, "A decentralized multiloop scheme for robust control of a power flow controller with two shunt modular multilevel converters," *IEEE Trans. Ind. Informat.*, vol. 14, no. 10, pp. 4309–4321, Oct. 2018.

[6] N. Zeb, B. Khan, S. M. Ali, C. A. Mehmood, R. Sajjad, U. Farid, and A. Bibi, "Adaptive controller based unified power flow control for low power oscillation damping," *Asian J. Control*, vol. 20, no. 3, pp. 1115–1124, May 2018.
[7] F. M. Albatsh, S. Mekhilef, S. Ahmad, and H. Mokhlis, "Fuzzy-logic-based UPFC and laboratory prototype validation for dynamic power flow control in transmission lines," *IEEE Trans. Ind. Electron.*, vol. 64, no. 12, pp. 9538–9548, Dec. 2017.
[8] F. Z. Peng, Y. Liu, S. Yang, S. Zhang, D. Gunasekaran, and U. Karki, "Transformer-less unified power-flow controller using the cascade multi-level inverter," *IEEE Trans. Power Electron.*, vol. 31, no. 8, pp. 5461–5472, Aug. 2016.
[9] C. Zheng and J. Wang, "The method of harmonic compensation of UPQC based on Euler–Lagrange model," in *Proc. IEEE 8th Int. Power Electron. Motion Control Conf. (IPEMC-ECCE Asia)*, Hefei, China, May 2016, pp. 142–146.
[10] G. Bergna-Diaz, D. Zonetti, S. Sanchez, R. Ortega, and E. Tedeschi, "PI passivity-based control and performance analysis of MMC multiterminal HVDC systems," *IEEE J. Emerg. Sel. Topics Power Electron.*, vol. 7, no. 4, pp. 2453–2466, Dec. 2019.
[11] V. Narasimhulu, D. V. A. Kumar, and C. S. Babu, "Fuzzy logic control of SLMMC-based SAPF under nonlinear loads," *Int. J. Fuzzy Syst.*, vol. 22, no. 2, pp. 428–437, Mar. 2020.
[12] E. Prieto-Araujo, A. Junyent-Ferré, G. Clariana-Colet, and O. Gomis-Bellmunt, "Control of modular multilevel converters under singular unbalanced voltage conditions with equal positive and negative sequence components," *IEEE Trans. Power Syst.*, vol. 32, no. 3, pp. 2131–2141, May 2017.
[13] S. Yiyan, Y. Bo, and S. Hongchun, "Passive current control design for MMC in HVDC systems through energy reshaping," *Electronics*, vol. 8, no. 9, pp. 96–102, Sep. 2019.
[14] O. D. Montoya, A. Garcés, and G. Espinosa-Pérez, "A generalized passivity-based control approach for power compensation in distribution systems using electrical energy storage systems," *J. Energy Storage*, vol. 16, pp. 259–268, Apr. 2018.
[15] F. Ma, Z. Zhu, J. Min, Y. Yue, and X. He, "Model analysis and sliding mode current controller for multilevel railway power conditioner under the V/v traction system," *IEEE Trans. Power Electron.*, vol. 34, no. 2, pp. 1243–1253, Feb. 2019.
[16] Q. Hou, S. Ding, X. Yu, and K. Mei, "A super-twisting-like fractional controller for SPMSM drive system," *IEEE Trans. Ind. Electron.*, vol. 69, no. 9, pp. 9376–9384, Sep. 2022.
[17] J. Kucka and A. Mertens, "Improved current control for a quasi-two-level PWM-operated modular multilevel converter," *IEEE Trans. Power Electron.*, vol. 35, no. 7, pp. 6842–6853, Jul. 2020.
[18] F. Qin, F. Gao, and C. Zhang, "Operational analyses and control scheme of nine-arm modular multilevel converter," *IEEE Trans. Power Electron.*, vol. 35, no. 4, pp. 3416–3433, Apr. 2020.
[19] Q. Yang, M. Saeedifard, and M. A. Perez, "Sliding mode control of the modular multilevel converter," *IEEE Trans. Ind. Electron.*, vol. 66, no. 2, pp. 887–897, Feb. 2019.
[20] C. Pazhanimuthu and S. Ramesh, "Grid integration of renewable energy sources (RES) for power quality improvement using adaptive fuzzy logic controller based series hybrid active power filter (SHAPF)," *J. Intell. Fuzzy Syst.*, vol. 35, no. 1, pp. 749–776, Jul. 2018.
[21] Y. Sang, B. Yang, W. Yao, and L. Jiang, "Design and implementation of perturbation observer-based robust passivity-based control for VSC-MTDC systems considering offshore wind power integration," *IET Gener., Transmiss. Distrib.*, vol. 12, no. 10, pp. 2415–2424, May 2018.
[22] J. Min, F. Ma, Q. Xu, Z. He, A. Luo, and A. Spina, "Analysis, design, and implementation of passivity-based control for multilevel railway power conditioner," *IEEE Trans. Ind. Informat.*, vol. 14, no. 2, pp. 415–425, Feb. 2018.
[23] J. Lai, X. Yin, L. Jiang, X. Yin, Z. Wang, and Z. Ullah, "Disturbance-observer-based PBC for static synchronous compensator under system disturbances," *IEEE Trans. Power Electron.*, vol. 34, no. 11, pp. 11467–11481, Nov. 2019.
[24] A. Jafari and G. Shahgholian, "Analysis and simulation of a sliding mode controller for mechanical part of a doubly-fed induction generator-based wind turbine," *IET Gener., Transmiss. Distrib.*, vol. 11, no. 10, pp. 2677–2688, Jul. 2017.
[25] M. Kchaou and H. Jerbi, "Reliable H_∞ and passive fuzzy observer-based sliding mode control for nonlinear descriptor systems subject to actuator failure," *Int. J. Fuzzy Syst.*, vol. 24, no. 1, pp. 105–120, Feb. 2022.
[26] Z. Li, C. Zang, P. Zeng, H. Yu, S. Li, and J. Bian, "Control of a grid-forming inverter based on sliding-mode and mixed H_2/H_∞ control," *IEEE Trans. Ind. Electron.*, vol. 64, no. 5, pp. 3862–3872, May 2017.
[27] M. A. Qureshi, I. Ahmad, and M. F. Munir, "Double integral sliding mode control of continuous gain four quadrant quasi-Z-source converter," *IEEE Access*, vol. 6, pp. 77785–77795, 2018.
[28] Q. Hou and S. Ding, "GPIO based super-twisting sliding mode control for PMSM," *IEEE Trans. Circuits Syst. II, Exp. Briefs*, vol. 68, no. 2, pp. 747–751, Feb. 2021.

CHANG JIANG received the B.S. degree in electrical engineering and automation from Anhui Jianzhu University, Hefei, China, in 2014, and the M.S. degree from the Shanghai University of Electric Power, Shanghai, China, in 2018. He is currently pursuing the Ph.D. degree in electrical engineering with Shanghai University. His research interests include power system automation and active power filters.

SHAOHUA ZHANG received the B.E. degree from Xian Jiaotong University, Xi'an, China, in 1988, the M.E. degree from the Shanghai University of Technology, Shanghai, China, in 1991, and the Ph.D. degree from Shanghai University, Shanghai, in 2001, all in electrical engineering. He was a Research Associate with The Hong Kong Polytechnic University, in 2004 and 2006. He is currently a Professor with Shanghai University. His research interests include power system economics, restructuring, and risk management.